DNA–histone H3 complex was incorporated and localized in endosomes and lysosomes as shown by colocalization with dextran and LysoTracker, respectively (Fig. 3e). Similarly to LL37, histone H3 and H4 allowed poly(C) and poly(A:U) to induce costimulation of naive CD4$^+$ T cells (Fig. 3f). These data indicated that NAs from self or pathogens could induce T-cell costimulation by forming complexes with antimicrobial peptides such as LL37 or core histones.

NA-mediated costimulation is independent of known sensors. To determine the mechanism of NA recognition and activation in T cells, we analysed the possible involvement of cytosolic sensors of NAs in innate cells. DNA-dependent activator of IRFs (DAI; also known as ZBP1) was first reported to function as a cytoplasmic DNA receptor[21]. Absent in melanoma 2 (AIM2) was identified as a cytosolic DNA sensor that activates inflammasome[22]. Stimulator of IFN genes (STING) and TBK1 have been identified as essential molecules that mediate a wide range of cytosolic DNA-induced type I IFN responses[23–25]. To examine the possible involvement of these sensors for T-cell costimulation, we tested naive CD4$^+$ T cells derived from *Zbp1*$^{-/-}$, *Asc*$^{-/-}$ (which links AIM2 to caspase-1), *Sting*$^{-/-}$ and *Tnf*$^{-/-}$ *Tbk1*$^{-/-}$ mice. However, surprisingly, DNA-mediated costimulation was induced normally in these T cells (Fig. 4a–c, Supplementary Fig. 3a), strongly suggesting that T cells utilize a DNA-sensing system different from innate immune cells.

TLR3 recognizes poly(I:C) in the endosome and initiates signalling through the adaptor, TRIF[1]. On the other hand, retinoic acid-inducible gene I (RIG-I) and melanoma differentiation-associated gene 5 (MDA5) sense poly(I:C) and viral RNA in the cytoplasm, which activates an adaptor, IFN-β promoter stimulator 1 (IPS-1; also known as MAVS)[26,27]. To examine the possibility that RIG-I/MDA5 and TLR3 may recognize RNA cooperatively or separately in T cells, we examined RNA-mediated T cell costimulation in IPS-1/TRIF-doubly deficient mice. Normal costimulation by poly(I:C) and poly(I) was observed in *Ips-1*$^{-/-}$ *Trif*$^{-/-}$ T cells (Fig. 4d). In addition, to determine the functional redundancy between TLRs and inflammasomes or RIG-I-like receptors (RLRs), we generated MyD88/ASC-and MyD88/IPS-1 doubly-deficient mice. NA-mediated costimulation was normally induced in naive CD4$^+$ T cells from both mutant mice (Supplementary Fig. 3b,c). It has been demonstrated that NAs are promiscuously sensed by HMGB proteins to induce type I IFN and pro-inflammatory cytokines[28]. However, downmodulation of all three HMGB proteins in CD4$^+$ T cells using small interfering RNA did not alter IL-2 production in response to NAs (Supplementary Fig. 3d).

To identify the mechanism underlying the NA-mediated costimulatory signal to induce IL-2 production in T cells, we

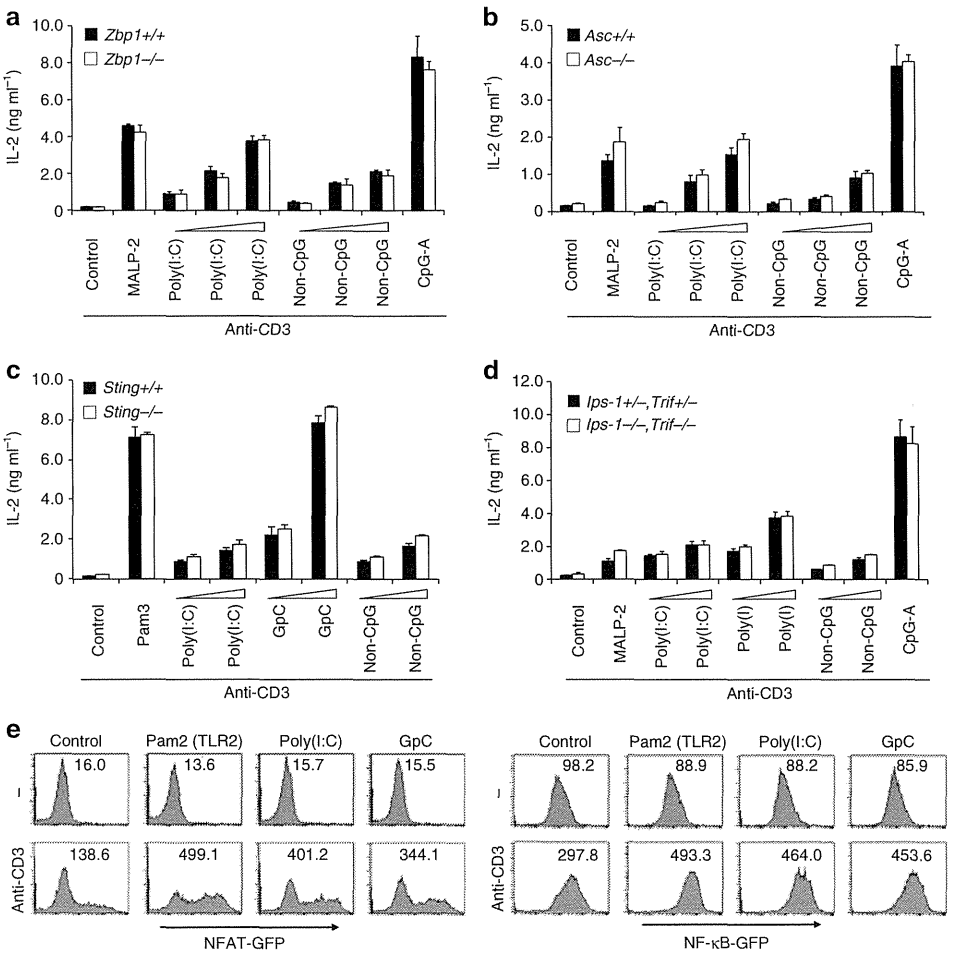

Figure 4 | NA-mediated T cell costimulation is independent of known innate sensors. (**a**–**d**) Naive CD4$^+$ T cells derived from WT or *Zbp1*$^{-/-}$ (**a**), *Asc*$^{-/-}$ (**b**), *Sting*$^{-/-}$ (**c**) or *Ips-1*$^{-/-}$ *Trif*$^{-/-}$ (**d**) mice were stimulated with plate-bound anti-CD3ε and the indicated ligands. After 48 h, IL-2 production was measured by ELISA. (**e**) T-cell hybridoma reporter cells expressing NFAT-GFP (left) or NF-κB-GFP (right) were stimulated with the indicated ligands with or without immobilized anti-CD3ε for 24 h and analysed by flow cytometry. Error bars indicate s.d. Data are representative of at least two independent experiments.

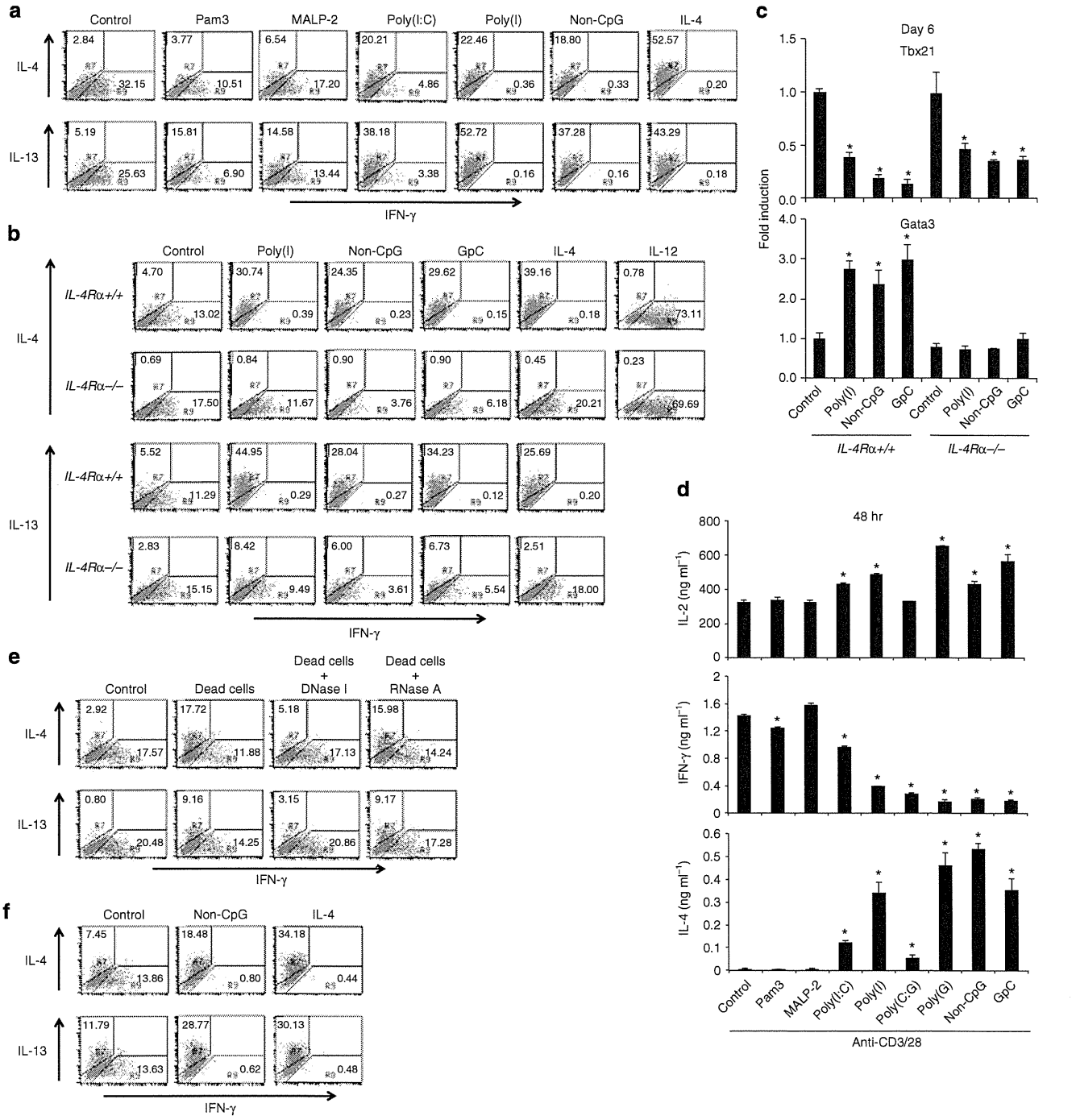

Figure 5 | NA-mediated costimulation induces Th2 differentiation. (**a**) Naive CD4$^+$ T cells were stimulated with immobilized anti-CD3ε (10 μg ml^{-1}) plus anti-CD28 (10 μg ml^{-1}) and the indicated ligands for 3 days, followed by culture with IL-2 (10 ng ml^{-1}) for an additional 3 days. Cells were subjected to real-time PCR analysis (**b**), or restimulated with immobilized anti-CD3ε plus anti-CD28 for 6 h for staining of intracellular cytokines IL-4 and IL-13. (**b**,**c**) Naive CD4$^+$ T cells from WT and IL-4Rα$^{-/-}$ mice were activated similarly as in (**a**) and cells were subjected to real-time PCR analysis (**c**) or restimulated with immobilized anti-CD3ε plus anti-CD28 for 6 h for staining of intracellular cytokines IL-4 and IL-13. *$P<0.05$, Student's *t*-test (compared with anti-CD3/CD28 plus non-CpG in WT cells). (**d**) Naive CD4$^+$ T cells were stimulated for 48 h with anti-CD3ε plus anti-CD28 and the indicated ligands and cytokine production was analysed by ELISA. *$P<0.05$, Student's *t*-test (compared with anti-CD3/CD28 alone). (**e**) Naive CD4$^+$ T cells with or without γ-irradiated naive CD4$^+$ T cells (Dead cells) at a 1:1 ratio were stimulated with anti-CD3ε plus anti-CD28 in the presence or absence of DNase I or RNase A, and analysed similarly as in (**a**). (**f**) Naive CD4$^+$ T cells from OT-II Tg mice were co-cultured with irradiated T cell-depleted splenocytes from C57BL/6 mice as APCs, together with OVA peptide (10 μM) in the presence or absence of non-CpG for 6 days. CD4$^+$ T cells were restimulated with immobilized anti-CD3ε plus anti-CD28 for 6 h for staining of intracellular cytokines. Error bars indicate s.d. Data are representative of at least three independent experiments.

analysed the activation of NF-κB and NFAT, both of which are essential for T-cell activation[29]. T-cell hybridoma (2B4) expressing the NF-κB-GFP or NFAT-GFP was stimulated by NAs plus anti-CD3. We observed that poly(I:C) and GpC markedly increased activation of NF-κB and NFAT, compared with anti-CD3 alone (Fig. 4e). These data suggest that enhanced

activation of NF-κB and NFAT is involved in the induction of NA-mediated T-cell costimulation. It is also worth noting that NA-induced costimulation of a T-cell hybridoma, which is definitely free of any innate cells, confirms that NA directly stimulates T cells.

NA-mediated costimulation induces Th2 cell differentiation. A recent study demonstrated that DNA released from dying host cells stimulates Th2 responses *in vivo*[30]. It is also reported that stimulation of RLRs by specific ligands biases the immune system toward a Th2 response, whereas the TLR signalling strongly induces Th1 and Th17 responses[31]. Accordingly, it seemed possible that NA-induced stimulation of T cells would induce Th2 cell differentiation. To test this hypothesis, naive $CD4^+$ T cells were stimulated *in vitro* with anti-CD3 plus anti-CD28 together with various NAs without blocking Abs against IFN-γ or IL-4. NAs such as poly(I:C), poly(I) and non-CpG strongly induced the differentiation of IL-4-producing T cells without the addition of exogenous IL-4 (Fig. 5a). By contrast, NAs strongly inhibited the differentiation of IFN-γ-producing T cells (Fig. 5a), and also increased the frequency of Th2 cells producing IL-5, IL-9, IL-13 and IL-10 (Fig. 5a, Supplementary Fig. 4a). Consistently, the expression of the Th2-master regulator GATA-3 was enhanced, whereas the expression of T-bet, the Th1-master regulator was strongly inhibited in the T cells cultured with NAs (Supplementary Fig. 4b), suggesting that NAs directly induce the differentiation of Th2 cells. Notably, unlike NAs, TLR2 ligands had a minimal effect on Th1 and Th2 differentiation (Fig. 5a), and NA-mediated costimulation did not affect the development of IL-17-producing T cells (Supplementary Fig. 4c). Since NAs induced Th2 differentiation of MyD88/TRIF-double deficient T cells similarly to control T cells (Supplementary Fig. 4d), this processes does not require TLR signalling.

The generation of Th2 cells is dependent on IL-4–STAT6 signalling, which leads to the upregulation of GATA-3 (ref. 32). We assessed whether Th2 differentiation induced by NA-mediated costimulation was also IL-4–STAT6-dependent. IL-4 receptor (R) α-deficient T cells after activation by NAs for 6 days failed to produce any Th2 cytokines including IL-4 and IL-13 (Fig. 5b). In addition, the induction of GATA-3 expression was severely diminished in IL-4Rα-deficient T cells (Fig. 5c). Similar results were obtained using *Stat6*$^{-/-}$ $CD4^+$ T cells (Supplementary Fig. 4e), indicating that NA-mediated Th2 differentiation requires IL-4–STAT6 signalling. However, NA-mediated inhibition of IFN-γ production and T-bet expression was still observed in IL-4Rα-deficient T cells (Fig. 5b,c), suggesting that NA-mediated inhibition of Th1 differentiation is independent of IL-4 signalling. Therefore, it is likely that NA-mediated costimulation may enhance IL-4 production at an early time point (within 48 h), which then induces Th2 differentiation. Indeed, IL-4 production was induced at 48 h by NAs but not TLR2 ligands, whereas IFN-γ production was reduced (Fig. 5d). NA-induced enhancement of IL-2 production was not strong upon stimulation with anti-CD3 plus CD28 as compared with anti-CD3 alone. Strong costimulation with anti-CD28 resulted in reduced enhancement, though significantly enhanced (Fig. 5d).

Collectively, these data demonstrate that NAs induce Th2 differentiation in an IL-4 signal-dependent manner similarly to the canonical Th2 differentiation pathway induced by exogenous IL-4, whereas suppression of Th1 differentiation by NAs is independent of IL-4 signalling.

We next determined whether self-DNA from dead cells induce Th2 differentiation. We found that the addition of dead cells (irradiated naive $CD4^+$ T cells or irradiated HEK 293 cells) to the T-cell culture enhanced the differentiation of IL-4-producing cells, which was cancelled by the addition of DNase I into the medium (Fig. 5e, Supplementary Fig. 5f). Addition of RNase A resulted in minimal effect. These data suggest that self-DNA is a critical factor for Th2 differentiation induced by dead cells. To examine whether NA-mediated Th2 differentiation is induced upon antigen stimulation, OVA-specific naive CD4+ T cells from OT-II Tg mice were stimulated with OVA peptide-pulsed irradiated splenocytes plus non-CpG. Non-CpG promoted Th2 differentiation under the condition, strongly suggesting that NAs induces T-cell costimulation even when T cells are activated by antigen-pulsed APCs (Fig. 5f).

Mechanisms underlying NA-induced Th2 differentiation. To determine the mechanism by which NAs induces Th2 differentiation, we compared the gene expression profiles in $CD4^+$ T cells activated under neutral conditions in the presence or absence of non-CpG. Surprisingly, before the upregulation of GATA-3, the expression of T-bet was strongly inhibited by non-CpG-mediated costimulation (Fig. 6a). Following the suppression of T-bet expression, the expression of Th2-associated genes was upregulated and IFN-γ was downregulated at 48 h after stimulation (Fig. 6a). We further confirmed that various NAs other than non-CpG also induced the suppression of T-bet and the upregulation of GATA-3 and IL-4 expression (Supplementary Fig. 5a). We then compared the kinetics of the expression of Th1/Th2-associated genes upon stimulation with IL-4 or non-CpG. GATA-3 was quickly induced in $CD4^+$ T cells by exogenous IL-4 (at 24 h), followed by the induction of Th2 cytokines and the inhibition of T-bet and IFN-γ expression. By contrast, in $CD4^+$ T cells stimulated with non-CpG, GATA-3 expression was induced after inhibition of T-bet expression, suggesting that Th2-associated genes are indirectly induced by non-CpG-mediated costimulation. In addition to these kinetic differences, inhibition of T-bet expression by non-CpG was more rapid and robust than by exogenous IL-4 (Fig. 6b). T-bet inhibits Th2 differentiation by directly inhibiting the expression of Th2 cytokines and sequestering GATA-3 from the promoters of Th2 cytokines[33]. Using ChIP analysis, we showed that the binding of GATA-3 to the IL-4 and IL-13 promoters was enhanced in $CD4^+$ T cells by stimulation with non-CpG (Fig. 6c). Therefore, it is likely that NA-mediated costimulation induces Th2 differentiation primarily by inhibiting T-bet expression.

To test this hypothesis further, we compared Th2 differentiation by the blockade of IFN-γ signalling and non-CpG stimulation, because the expression of T-bet is controlled by IFN-γ signalling[34]. We found that the T-bet expression in $CD4^+$ T cells cultured in the presence of anti-IFN-γ was much lower than those stimulated with non-CpG at early time point (48 h) after TCR stimulation (Fig. 6d). However, the expression of GATA-3 and Th2 cytokines in T cells cultured with anti-IFN-γ was much lower than those stimulated with non-CpG (Fig. 6d), suggesting that inhibition of T-bet expression by non-CpG is not sufficient, though partially contributes, for the upregulation of Th2-associated gene expression. Additional signal(s) are required for the induction of Th2-associated genes by non-CpG-mediated costimulation. Consistently, the Th2 polarization by the presence of anti-IFN-γ was weaker than by non-CpG later (day 6) after TCR priming (Fig. 6e). Thus, non-CpG-mediated costimulation simultaneously inhibits T-bet expression and enhances the expression of Th2-associated genes.

As T-bet controls Th1 development by directly activating IFN-γ (ref. 34), it is likely that NA-mediated costimulation would inhibit Th1 development under Th1-polarizing conditions. As expected, non-CpG inhibits Th1 development and

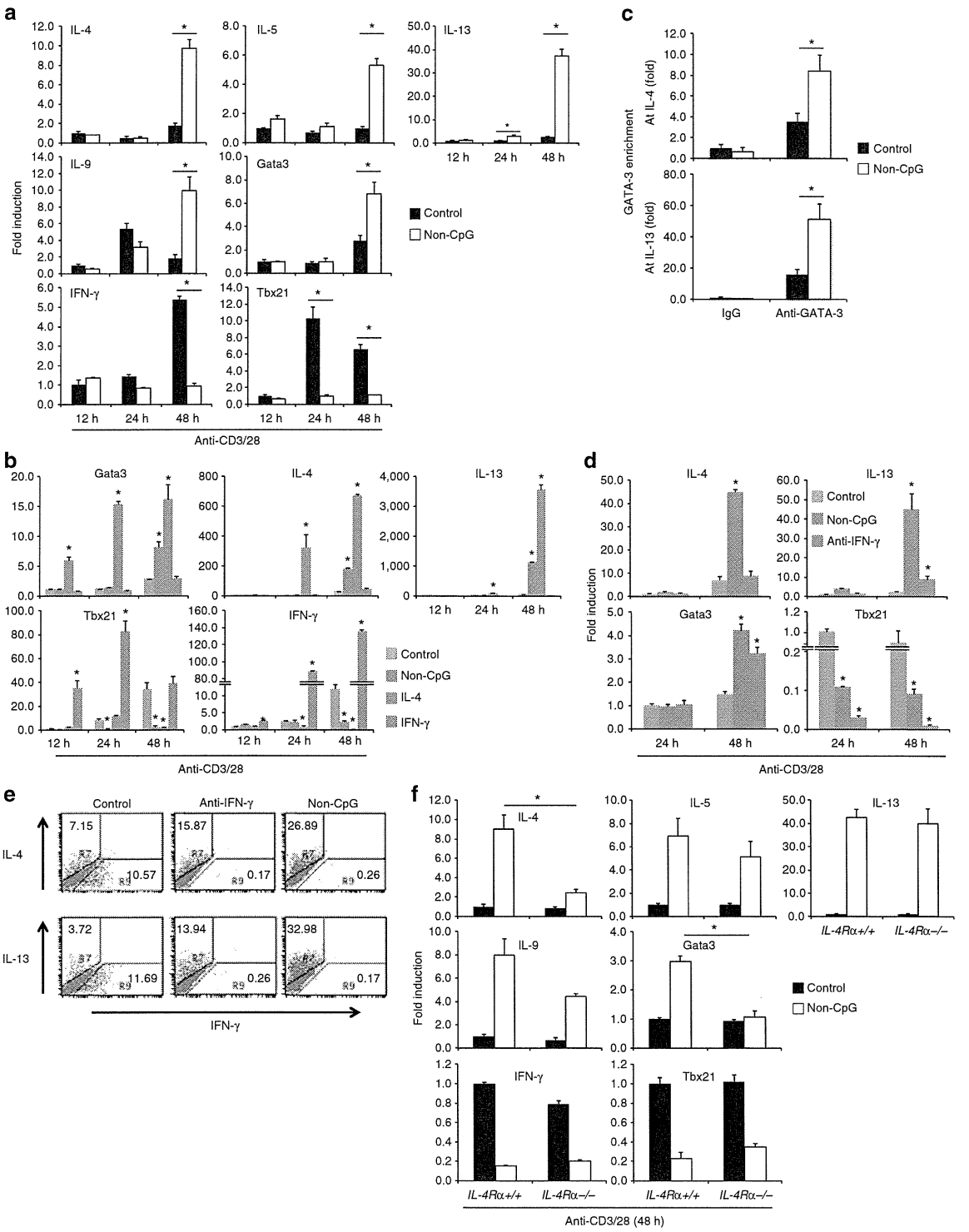

Figure 6 | Molecular mechanism of NA-mediated Th2 differentiation. (**a**) Naive CD4$^+$ T cells were stimulated with anti-CD3ε plus anti-CD28 with or without non-CpG for the indicated periods and mRNA expression was analysed by real-time PCR. *$P<0.01$, Student's *t*-test (compared with anti-CD3/CD28 alone). (**b**) Naive CD4$^+$ T cells were stimulated by NAs or IL-4 and analysed similarly in (**a**). *$P<0.01$, Student's *t*-test (compared with anti-CD3/CD28 alone). (**c**) Naive CD4$^+$ T cells were stimulated with anti-CD3ε plus anti-CD28 together with non-CpG for 48 h, and ChIP analyses were performed by immunoprecipitation with control Ab (IgG) or anti-GATA-3. Quantitative PCR analysis of the GATA3 binding at the IL-4 and IL-13 gene promoters. The results were normalized to those of a standardized aliquot of input chromatin. *$P<0.05$, Student's *t*-test (compared with anti-CD3/CD28 alone). (**d**,**e**) Naive CD4$^+$ T cells were stimulated in the presence of non-CpG or anti-IFN-γ Ab and mRNA expression (**d**) and intracellular cytokine expression (day 6) (**e**) were analysed. *$P<0.01$, Student's *t*-test (compared with anti-CD3/CD28 alone). (**f**) Naive CD4$^+$ T cells from WT and IL-4Rα$^{-/-}$ mice were stimulated and analysed similarly in (**a**). *$P<0.01$, Student's *t*-test (compared with anti-CD3/CD28 plus non-CpG in WT cells). Error bars indicate s.d. Data are representative of at least two independent experiments.

IFN-γ production even under Th1 differentiation condition (Supplementary Fig. 5b).

We then analysed whether IL-4 signalling is required for the early expression of Th2-associated genes after NA-mediated costimulation. Interestingly, the augmentation of the expression of IL-4 and GATA-3 by non-CpG was severely impaired in IL-4Rα-deficient $CD4^+$ T cells, whereas the upregulation of IL-5, IL-9 and IL-13 expression and downregulation of IFN-γ and T-bet expression was largely unaffected (Fig. 6f). Similar results were obtained in the *Stat6*$^{-/-}$ $CD4^+$ T cells (Supplementary Fig. 5c). These data suggest that non-CpG-mediated T-cell costimulation directly induced the expression of IL-5, IL-9 and IL-13, partly through the inhibition of T-bet expression, whereas IL-4 and GATA-3 expression was induced by IL-4–STAT6 signalling. Naive $CD4^+$ T cells are capable of producing IL-4 upon primary TCR stimulation in the absence of exogenous IL-4, and the early IL-4 is rapidly consumed by the $CD4^+$ T cells themselves[35]. Therefore, NA-mediated IL-4 production may require early IL-4 autocrine signalling to induce the autoactivation of GATA-3 expression. Notably, however, expression of all Th2-associated genes in IL-4Rα-deficient $CD4^+$ T cells disappeared by day 6 after priming with NAs. Although non-CpG stimulation induces the enrichment of GATA-3 on the IL-13 promoter (Fig. 6c), it seems that early induction of IL-13 expression by non-CpG (at 48 h) is independent of GATA-3 because IL-13 expression was enhanced by non-CpG in IL-4Rα-deficient $CD4^+$ T cells despite the lack of GATA-3 upregulation by non-CpG (Fig. 6f). However, it seems that the enrichment of GATA-3 on the IL-13 promoter is critical for IL-13 expression later (in day 6) after TCR priming for its maintenance because the induction of IL-13 and GATA-3 expression by non-CpG was diminished later after TCR priming (in day 6) in IL-4Rα-deficient $CD4^+$ T cells (Fig. 5b,c). These data indicate that autocrine IL-4 is required for the induction of IL-4 and GATA-3 upon non-CpG stimulation, which then acts to amplify and stabilize the expression of Th2-associated genes.

Discussion

The present study shows that NAs directly stimulate $CD4^+$ T cells through a NA sensor different from those of the innate system, subsequently leading to Th2 cell differentiation. In addition to TLRs, a growing number of NA sensors have been identified in the innate immune system, including RLRs, IPS-1-dependent sensors, MyD88/TRIF-dependent sensors, ASC-dependent inflammasomes and STING-dependent sensors[36]. However, we found that recognition of NAs by T cells is independent of all of these known sensors including HMGBs, although we cannot conclusively exclude the possibility that some known NA sensors work redundantly.

We found that a higher-order structure of the NAs is required for their incorporation by T cells. Since T cells can incorporate genomic self-DNA only when it is complexed with antimicrobial peptides or core histones, T cells may respond to NAs from dying cells at the site of inflammation and infection, where antimicrobial peptides and/or histones are released. We also demonstrated that specific recognition and uptake of RNA induces costimulatory responses. A recent study demonstrated that cells infected with several viruses including vaccinia virus contained higher-order structured RNA that stimulated MDA5 (ref. 37), indicating the possibility that T cells may recognize such viral RNA and are activated. Recent studies demonstrated that, upon infection with nonpermissive HIV, cytoplasmic DNA derived from incomplete reverse transcripts caused $CD4^+$ T cell death through recognition of the cytosolic DNA by a sensor IFI16 followed by activation of the ASC-caspase-1 pathway[38,39]. It was also reported that transfected DNA was colocalized with IFI16 in activated T cells[40]. However, our result that DNA-mediated costimulation was normally induced in ASC-deficient $CD4^+$ T cells suggests that IFI16 is not involved in the DNA-mediated costimulation in T cells. While cytosolic DNA stimulates IFI16 upon HIV infection or DNA transfection, incorporated DNAs are accumulated in endosome/lysosome and induce T-cell costimulation in our experiments without activation of IFI16 probably due to the failure to deliver DNA to the cytosol.

Furthermore, a recent study showed that immunization with RLR ligands or infection with viruses, which mainly activate RLRs, results in enhanced Th2 responses and much weaker Th1 responses[31], supporting our observation that NAs directly stimulate the induction of Th2 responses. It is known that TLR stimulation of innate immune cells promotes Th1 and Th17 responses by inducing the Th1-polarizing cytokine IL-12 and the Th17-polarizing cytokines IL-6/IL-23/IL-1 (refs 1,41). Recent studies, including ours, show that TLR2 ligands directly activate Th1 but not Th2 cells[7] and promote Th17 differentiation[8]. In contrast to TLR, the activation of RLRs suppresses Th1 and Th17 differentiation through the inhibition of IL-12 and IL-23 production, resulting in the enhanced differentiation of Th2 cells[31]. Our results demonstrate that direct stimulation of T cells by NAs strongly inhibit the initial expression of T-bet, which allows the initial production of IL-4 and Th2 cytokines to induce Th2 differentiation. Thus, similar to Th1 and Th17 responses induced by TLRs in innate cells and T cells, it is likely that activation of RLRs in innate cells and the NA sensor in T cells by NAs cooperatively induces Th2 differentiation.

The initial origin of IL-4 to trigger Th2 differentiation has been extensively analysed but remains unclear. It has been reported that basophils serve as Th2 cell-promoting APCs by producing IL-4 and/or thymic stromal lymphopoietin[14]. However, their role as APCs remains controversial[42]. It has been suggested that naive T cells are a possible source of IL-4 (refs 43,44), which modestly induces Th2 differentiation when IFN-γ and IL-12 are neutralized[35]. Although it has been proposed that Th2 differentiation may occur as a default pathway, $CD4^+$ T cells in IL-12 p40-deficient mice fail to differentiate into Th2 cells in response to intracellular pathogens[45]. Thus, the simple blocking of Th1-inducing stimuli such as IL-12 or IFN-γ is not sufficient to induce Th2 differentiation, suggesting the existence of additional Th2-inducing factors. However, such factors for the initial triggering of IL-4 production from naive $CD4^+$ T cells under physiological conditions have not been identified. We here provide strong evidence that the initial IL-4 production derived from naive $CD4^+$ T cells upon recognition of NAs in the absence of any exogenous cytokines or neutralizing antibodies instructs naive $CD4^+$ T cells to differentiate into Th2 cells.

A recent report demonstrated that aluminium hydroxide adjuvant (alum) causes cell death and release of host DNA at sites of immunization, which mediates the adjuvant effect for Th2-biased adaptive responses[30]. As the mechanism to induce Th2 responses, it has been reported that uric acid released in the peritoneal cavity after injection of alum may have a role in promoting Th2 cell responses independently of the ASC inflammasome or TLR signalling[46]. As uric acid crystals released at the sites of immunization/inflammation induce extracellular DNA traps formation by neutrophil, eosinophil and basophil[47], uric acid-induced extracellular DNA traps may directly stimulate T cells to induce Th2 response. A recent study reported that defects in clearance of apoptotic airway epithelial cells upon environmental allergen encounter lead to augmented Th2 cytokine production and airway hyper-responsiveness[48], indicating that *in vivo* Th2 responses are closely related to host

cell death accompanied by host DNA release. In line with the hypothesis, we found that self-DNA from dead cells induces Th2 differentiation.

Collectively, we have identified NAs as a direct Th2-inducing factor, which induces initial production of IL-4 by naive CD4$^+$ T cells, which in turn induces Th2 differentiation. Although we have not identified the NAs sensor in T cells yet, our results provide the possibility that NAs may be critical targets for the development of improved vaccine adjuvants and the overall design of therapeutics to control allergic diseases.

Methods

Mice. C57BL/6 mice were purchased from Clea Japan, Inc. The mice deficient in MyD88, TRIF-deficient, IPS-1 ZBP1 and STAT6 were provided by Dr Akira S. *Asc*$^{-/-}$ mice were provided by Dr Taniguchi S and Dr Noda T. *Sting*$^{-/-}$ and *Il4ra*$^{-/-}$ mice were provided by Dr Barber GN and Dr Brombacher F, respectively. Mice aged 8–16 weeks were used. All mice were maintained under specific pathogen-free conditions and all experiments were conducted under protocols approved by RIKEN Yokohama Institute.

ELISA and cell growth analysis. Cell culture supernatants were analysed by ELISA for the production of IL-2 (BD biosciences), IL-4 (BD biosciences) and IFN-γ (BD biosciences). Cell growth was assessed by the MTS assay-based Cell Counting Kit-8 (DOJINDO).

Helper T-cell differentiation. CD4$^+$/CD25$^-$/CD62L$^+$/NK1.1$^-$ (naive) T cells were isolated from spleens using a FACS-Aria cell sorter. For Th0 cells, cells were stimulated with plate-bound anti-CD3 (2C11, 10 μg ml^{-1}) and anti-CD28 (PV-1, 10 μg ml^{-1}) Abs in the presence of the indicated ligands. For Th1 cells, cells were cultured in the presence of IL-12 (10 ng ml^{-1}) and anti-IL-4 Abs (10 μg ml^{-1}). For Th2 cells, cells were similarly cultured in the presence of IL-4 (10 ng ml^{-1}).

Real-time quantitative PCR. After removal of genomic DNA by treatment with DNase (Wako Nippon Gene), randomly primed cDNA strands were generated with reverse transcriptase II (Invitrogen). RNA expression was quantified by real-time PCR with the following gene-specific primers and values were normalized to the expression of *Rps18* mRNA (Supplementary Table 2).

Reagents and Abs. The TLR2 ligands *N*-palmitoyl-*S*-(2,3-bis(palmitoyloxy)-(2*RS*)-propyl)-Cys-Ser-Lys$_4$ (Pam3) and macrophage-activating lipopeptide 2 (MALP-2) were purchased from EMC Microcollections. Poly(I:C), a TLR3 ligand, and LPS (*Escherichia. coli* O111:B4), a TLR4 ligand, were obtained from GE Healthcare Biosciences and Sigma, respectively. Flagellin, a TLR5 ligand, and loxoribine, a TLR7 ligand, were obtained from InvivoGen. Oligo DNAs including TLR9 ligands were purchased from Hokkaido System Science. Poly(A), poly(U), poly(C), poly(G), poly(I), poly(A:U) and poly(C:G) were purchased from Sigma. Calf thymus DNA and *E. coli* DNA was from Sigma and Invivogen, respectively. LL37 was from AnaSpec. Histone H1, H2A, H2B, H3 and H4 were from New England BioLabs. LL37 or histones were first premixed with genomic DNA (peptide:DNA mass ratio of 2:1). After 30-min incubation at room temperature, the mix was added to the T-cell cultures (final concentration was 10 μg ml^{-1} of DNA).

Abs specific for anti-IL-4 PE (11B11, 1:25 dilution) and anti-IFN-γ FITC (XMG1.2, 1:25 dilution) were obtained from BD Biosciences; anti-IL-5 PE (TRFK5, 1:25 dilution), anti-IL-10 PE (1:25 dilution) and anti-IL-13 PE (eBio13A, 1:25 dilution) from eBioscience; anti-IL-9 PE (RM9A4, 1:25 dilution) from BioLegend. ChIP analysis used mAb to GATA-3 (HG3-31AC; Santa Cruz, 1:125 dilution).

Intracellular cytokine staining analysis. CD4$^+$ T cells were restimulated with immobilized anti-CD3 and anti-CD28 for 6 h in the presence of 2 μM monensin (Sigma, St Louis, MO). Cells were fixed with 4% paraformaldehyde and permeabilized with 0.5% Triton X-100. After blocking with 3% BSA-PBS, cells were stained with antibodies to each cytokine. Flow cytometric analysis was performed on a FACSCalibur and data were analysed with BD CellQuest.

Cellular uptake of NA. To analyse the uptake of NA, 2×10^5 cells were pre-incubated at 37 °C for 10 min in medium. Cells were incubated with fluorescence-labelled NA at 37 °C for 90 min. Then cells were washed once in HANKS/0.1% BSA followed by an acidic wash with 100 mM acetic acid, 150 mM NaCl (pH2.7) for 1 min to remove unbound and cell surface-bound NA. Subsequently, cells were washed two times in HANKS/0.1% BSA, and were analysed by flow cytometry using the FACSCalibur.

Reporter cells. The 2B4–NFAT-GFP cells have been described[49] and the 2B4-NF-kB-GFP cells were established by transfection of NF-κB-GFP into 2B4 hybridoma cells. These cells were cultured in RPMI 1640 medium supplemented with 10% (vol/vol) FCS and β-mercaptoethanol.

Chromatin immunoprecipitation assay. Cells were fixed for 10 min at 4 °C with 10% formaldehyde. After incubation, glycine was added to a final concentration of 0.125 M to quench the formaldehyde. Cells were pelleted, washed three times with ice-cold PBS and then lysed. The lysates were sonicated to reduce DNA length to between 200 and 300 base pairs. The chromatin was pre-cleared with protein G agarose beads for 6 h and then incubated with 4 μg of anti-GATA-3 (HG3-31) agarose conjugate antibody (Santa Cruz, sc-268 AC) or control IgG overnight. The precipitates were washed and eluted in 120 μl of $NaHCO_3$ buffer with 1% SDS. The samples were treated with RNase and Proteinase K and then de-crosslinked at 65 °C overnight. Precipitated DNA was further purified with Qiaquick PCR purification kit (Qiagen) and was analysed by quantitative PCR (Supplementary Table 2)[50].

Confocal microscopic imaging. Cells were settled on glass-bottom, 35-mm tissue culture dishes (MATSUNAMI GLASS). Confocal microscopy analyses were performed with a Leica TCS SP5 confocal microscope with an oil immersion objective (HCX PL APO × 63/1.40–0.60 NA, Leica). Dual-color images were acquired using a sequential acquisition mode to avoid cross-excitation. To visualize the Histone–calf thymus DNA complex in CD4$^+$ T cells, calf thymus DNA (Sigma) was labelled with Cy5 using the Label IT Nucleic Acid Labelling Reagents (Mirus) and histone H3 was labelled with DyLight 488 using the antibody labelling kit (Pierce), according to the standard protocol provided by the respective manufacturers.

RNA interference. Double-stranded oligonucleotides corresponding to the target sequences were cloned into the pSuper.Retro RNAi plasmid (OligoengineInc.). The siRNA targeting sequences which function for commonly all three murine HMGB1/2/3 are 5′-GAGAAGTATGAGAAGGATATT-3′ and 5′-AAGTATGAGA AGGATATTGCT-3′.

Statistics. Statistical significance was determined by a two-tailed unpaired Student's *t*-test. $P<0.05$ was considered statistically significant.

References

1. Takeda, K., Kaisho, T. & Akira, S. Toll-like receptors. *Annu. Rev. Immunol.* **21,** 335–376 (2003).
2. Medzhitov, R. Toll-like receptors and innate immunity.. *Nat. Rev. Immunol.* **1,** 135–145 (2001).
3. Komai-Koma, M., Jones, L., Ogg, G. S., Xu, D. & Liew, F. Y. TLR2 is expressed on activated T cells as a costimulatory receptor. *Proc. Natl Acad. Sci. USA* **101,** 3029–3034 (2004).
4. Cottalorda, A. *et al.* TLR2 engagement on CD8 T cells lowers the threshold for optimal antigen-induced T cell activation. *Eur. J. Immunol.* **36,** 1684–1693 (2006).
5. Sutmuller, R. P. *et al.* Toll-like receptor 2 controls expansion and function of regulatory T cells. *J. Clin. Invest.* **116,** 485–494 (2006).
6. Liu, H., Komai-Koma, M., Xu, D. & Liew, F. Y. Toll-like receptor 2 signaling modulates the functions of CD4+ CD25+ regulatory T cells. *Proc. Natl Acad. Sci. U. S. A.* **103,** 7048–7053 (2006).
7. Imanishi, T. *et al.* Cutting edge: TLR2 directly triggers Th1 effector functions. *J. Immunol.* **178,** 6715–6719 (2007).
8. Reynolds, J. M. *et al.* Toll-like receptor 2 signaling in CD4(+) T lymphocytes promotes T helper 17 responses and regulates the pathogenesis of autoimmune disease. *Immunity* **32,** 692–702 (2010).
9. Caron, G. *et al.* Direct stimulation of human T cells via TLR5 and TLR7/8: flagellin and R-848 up-regulate proliferation and IFN-gamma production by memory CD4+ T cells. *J. Immunol.* **175,** 1551–1557 (2005).
10. Gelman, A. E. *et al.* The adaptor molecule MyD88 activates PI-3 kinase signaling in CD4+ T cells and enables CpG oligodeoxynucleotide-mediated costimulation. *Immunity* **25,** 783–793 (2006).
11. Gelman, A. E., Zhang, J., Choi, Y. & Turka, L. A. Toll-like receptor ligands directly promote activated CD4+ T cell survival. *J. Immunol.* **172,** 6065–6073 (2004).
12. Peng, G. *et al.* Toll-like receptor 8-mediated reversal of CD4+ regulatory T cell function. *Science* **309,** 1380–1384 (2005).
13. Zhu, J., Yamane, H. & Paul, W. E. Differentiation of effector CD4 T cell populations (*). *Annu. Rev. Immunol.* **28,** 445–489 (2010).
14. Paul, W. E. & Zhu, J. How are T(H)2-type immune responses initiated and amplified? *Nat. Rev. Immunol.* **10,** 225–235 (2010).
15. Kerkmann, M. *et al.* Spontaneous formation of nucleic acid-based nanoparticles is responsible for high interferon-alpha induction by CpG-A in plasmacytoid dendritic cells. *J. Biol. Chem.* **280,** 8086–8093 (2005).
16. Bishop, J. S. *et al.* Intramolecular G-quartet motifs confer nuclease resistance to a potent anti-HIV oligonucleotide. *J. Biol. Chem.* **271,** 5698–5703 (1996).

17. Dalpke, A. H., Zimmermann, S., Albrecht, I. & Heeg, K. Phosphodiester CpG oligonucleotides as adjuvants: polyguanosine runs enhance cellular uptake and improve immunostimulative activity of phosphodiester CpG oligonucleotides *in vitro* and *in vivo*. *Immunology* **106,** 102–112 (2002).
18. Arnott, S., Chandrasekaran, R. & Marttila, C. M. Structures for polyinosinic acid and polyguanylic acid. *Biochem. J.* **141,** 537–543 (1974).
19. Lande, R. *et al.* Plasmacytoid dendritic cells sense self-DNA coupled with antimicrobial peptide. *Nature* **449,** 564–569 (2007).
20. Mantovani, A., Cassatella, M. A., Costantini, C. & Jaillon, S. Neutrophils in the activation and regulation of innate and adaptive immunity. *Nat. Rev. Immunol.* **11,** 519–531 (2011).
21. Takaoka, A. *et al.* DAI (DLM-1/ZBP1) is a cytosolic DNA sensor and an activator of innate immune response. *Nature* **448,** 501–505 (2007).
22. Hornung, V. *et al.* AIM2 recognizes cytosolic dsDNA and forms a caspase-1-activating inflammasome with ASC. *Nature* **458,** 514–518 (2009).
23. Ishikawa, H. & Barber, G. N. STING is an endoplasmic reticulum adaptor that facilitates innate immune signalling. *Nature* **455,** 674–678 (2008).
24. Ishikawa, H., Ma, Z. & Barber, G. N. STING regulates intracellular DNA-mediated, type I interferon-dependent innate immunity. *Nature* **461,** 788–792 (2009).
25. Ishii, K. J. *et al.* A Toll-like receptor-independent antiviral response induced by double-stranded B-form DNA. *Nat. Immunol.* **7,** 40–48 (2006).
26. Kato, H. *et al.* Length-dependent recognition of double-stranded ribonucleic acids by retinoic acid-inducible gene-I and melanoma differentiation-associated gene 5. *J. Exp. Med.* **205,** 1601–1610 (2008).
27. Kawai, T. *et al.* IPS-1, an adaptor triggering RIG-I- and Mda5-mediated type I interferon induction. *Nat. Immunol.* **6,** 981–988 (2005).
28. Yanai, H. *et al.* HMGB proteins function as universal sentinels for nucleic-acid-mediated innate immune responses. *Nature* **462,** 99–103 (2009).
29. Smith-Garvin, J. E., Koretzky, G. A. & Jordan, M. S. T cell activation. *Annu. Rev. Immunol.* **27,** 591–619 (2009).
30. Marichal, T. *et al.* DNA released from dying host cells mediates aluminum adjuvant activity. *Nat. Med.* **17,** 996–1002 (2011).
31. Negishi, H. *et al.* Cross-interference of RLR and TLR signaling pathways modulates antibacterial T cell responses. *Nat. Immunol.* **13,** 659–666 (2012).
32. Zheng, W. & Flavell, R. A. The transcription factor GATA-3 is necessary and sufficient for Th2 cytokine gene expression in CD4 T cells. *Cell* **89,** 587–596 (1997).
33. Hwang, E. S., Szabo, S. J., Schwartzberg, P. L. & Glimcher, L. H. T helper cell fate specified by kinase-mediated interaction of T-bet with GATA-3. *Science* **307,** 430–433 (2005).
34. Afkarian, M. *et al.* T-bet is a STAT1-induced regulator of IL-12R expression in naive CD4+ T cells. *Nat. Immunol.* **3,** 549–557 (2002).
35. Noben-Trauth, N., Hu-Li, J. & Paul, W. E. Conventional, naive CD4+ T cells provide an initial source of IL-4 during Th2 differentiation. *J. Immunol.* **165,** 3620–3625 (2000).
36. Desmet, C. J. & Ishii, K. J. Nucleic acid sensing at the interface between innate and adaptive immunity in vaccination. *Nat. Rev. Immunol.* **12,** 479–491 (2012).
37. Pichlmair, A. *et al.* Activation of MDA5 requires higher-order RNA structures generated during virus infection. *J. Virol.* **83,** 10761–10769 (2009).
38. Monroe, K. M. *et al.* IFI16 DNA sensor is required for death of lymphoid CD4 T cells abortively infected with HIV. *Science* **343,** 428–432 (2014).
39. Doitsh, G. *et al.* Cell death by pyroptosis drives CD4 T-cell depletion in HIV-1 infection. *Nature* **505,** 509–514 (2014).
40. Berg, R. K. *et al.* T cells detect intracellular DNA but fail to induce Type I IFN responses: implications for restriction of HIV replication. *PloS One* **9,** e84513 (2014).
41. Goriely, S., Neurath, M. F. & Goldman, M. How microorganisms tip the balance between interleukin-12 family members. *Nat. Rev. Immunol.* **8,** 81–86 (2008).
42. Kim, S. *et al.* Cutting edge: basophils are transiently recruited into the draining lymph nodes during helminth infection via IL-3, but infection-induced Th2 immunity can develop without basophil lymph node recruitment or IL-3. *J. Immunol.* **184,** 1143–1147 (2010).
43. Yagi, R. *et al.* The IL-4 production capability of different strains of naive CD4(+) T cells controls the direction of the T(h) cell response. *Int. Immunol.* **14,** 1–11 (2002).
44. Liu, Z. *et al.* IL-2 and autocrine IL-4 drive the *in vivo* development of antigen-specific Th2 T cells elicited by nematode parasites. *J. Immunol.* **174,** 2242–2249 (2005).
45. Jankovic, D. *et al.* In the absence of IL-12, CD4(+) T cell responses to intracellular pathogens fail to default to a Th2 pattern and are host protective in an IL-10(-/-) setting. *Immunity* **16,** 429–439 (2002).
46. Kool, M. *et al.* An unexpected role for uric acid as an inducer of T helper 2 cell immunity to inhaled antigens and inflammatory mediator of allergic asthma. *Immunity* **34,** 527–540 (2011).
47. Schorn, C. *et al.* Monosodium urate crystals induce extracellular DNA traps in neutrophils, eosinophils, and basophils but not in mononuclear cells. *Front. Immunol.* **3,** 277 (2012).
48. Juncadella, I. J. *et al.* Apoptotic cell clearance by bronchial epithelial cells critically influences airway inflammation. *Nature* **493,** 547–551 (2013).
49. Ohtsuka, M. *et al.* NFAM1, an immunoreceptor tyrosine-based activation motif-bearing molecule that regulates B cell development and signaling. *Proc. Natl Acad. Sci. USA* **101,** 8126–8131 (2004).
50. Tanaka, S. *et al.* The enhancer HS2 critically regulates GATA-3-mediated Il4 transcription in T(H)2 cells. *Nat. Immunol.* **12,** 77–85 (2011).

Acknowledgements

We thank S. Yamasaki, T. Yokosuka, S. Tsukumo, A. Takeuchi, R. Onishi, H. Ike, Y. Motomura and M. Kubo for discussions and experimental help, M. Sakuma, M. Unno and A. Fujii for technical support, and H. Yamaguchi, M. Yoshioka and S. Kato for secretarial assistance. This work was supported by a Grant-in-Aid for Scientific Research from the Ministry of Education, Culture, Sports, Science and Technology of Japan (JSPS KAKENHI Grant numbers 24790489 for T.I. and 24229004 for T.S.).

Authors contributions

T.I. designed and performed the experiments and wrote the paper; C.I., M.E.S.G.B., Y.K., A.H-T. and H.H performed the experiments; T.K., O.T., K.J.I., S.T., T.N., F.B., G.N.B. and S.A. provided knockout mice; T.S. designed the experiments and wrote the paper.

Additional information

Supplementary Information accompanies this paper at http://www.nature.com/naturecommunications

Competing financial interests: The authors declare no competing financial interests.

Reprints and permission information is available online at http://npg.nature.com/reprintsandpermissions/

How to cite this article: Imanishi, T. *et al.* Nucleic acid sensing by T cells initiates Th2 cell differentiation. *Nat. Commun.* 5:3566 doi: 10.1038/ncomms4566 (2014).

DOI 10.1002/pmic.201300237 *Proteomics* 2014, *14*, 116–120

DATASET BRIEF

Phosphoproteome analysis of *Lotus japonicus* seeds

Yoko Ino[1], Akiyo Ishikawa[1], Ayako Nomura[1], Hideyuki Kajiwara[2], Kyuya Harada[2] and Hisashi Hirano[1]

[1] Advanced Medical Research Center, Yokohama City University, Yokohama, Japan
[2] Agrogenomics Research Center, National Institute of Agrobiological Sciences, Tsukuba, Japan

In this study, we report the first dataset of phosphoproteins of the seeds of a model plant, *Lotus japonicus*. This dataset might be useful in studying the regulatory mechanisms of seed germination in legume plants. By proteomic analysis of seeds following water absorption, we identified a total of 721 phosphopeptides derived from 343 phosphoproteins in cotyledons, and 931 phosphopeptides from 473 phosphoproteins in hypocotyls. Kinase-specific prediction analyses revealed that different kinases were activated in cotyledons and hypocotyls. In particular, many peptides containing ATM-kinase target motifs, X-X-pS/pT-Q-X-X, were detected in cotyledons. Moreover, by real-time RT-PCR analysis, we found that expression of a homolog of ATM kinase is upregulated specifically in cotyledons, suggesting that this ATM-kinase homolog plays a significant role in cell proliferation in the cotyledons of *L. japonicus* seeds. The data have been deposited to the ProteomeXchange with identifier PXD000053 (http://proteomecentral.proteomexchange.org/dataset/PXD000053).

Received: June 17, 2013
Revised: September 30, 2013
Accepted: October 28, 2013

Keywords:
Legume / *Lotus japonicus* / MS / Phosphoprotein / Plant proteomics

Elucidation of the regulatory mechanisms of germination is essential in order to increase agricultural productivity. In this effort, analyses of signaling pathways are considered to be indispensable. In *Arabidopsis thaliana*, Umezawa et al. [1] showed that phosphorylation by SNF1-related protein kinase 2 and dephosphorylation by protein phosphatase 2C are involved in abscisic acid signaling, which regulates germination. In rice, Assmann et al. [2] reported that a guanine nucleotide binding protein is related to gibberellic acid signaling, which also regulates germination. In legumes, however, there have been few reports describing the regulation of seed germination at the protein level.

Lotus japonicus is a model legume because of its small genome size, short life cycle, and synteny with other legume species [3]. In 2008, the complete nucleotide sequence of the *L. japonicus* genome has been determined, and a database has been constructed [4]. Consequently, it is now possible to perform genome database driven proteome analysis in this organism. Meanwhile, the development of high-performance MS and phosphopeptide-enrichment techniques such as IMAC and metal oxide affinity chromatography (MOAC) [5–8] have made it possible to comprehensively analyze phosphoproteins by MS. In this study, using the genome database and these analytical techniques, we profiled phosphoprotein expression in the cotyledons and hypocotyls of *L. japonicus* seeds after absorption of water.

After water absorption for 6 h, de-hulled seeds of *L. japonicus* (Regel) Larsen Miyakojima MG-20 were separated into cotyledons and hypocotyls. Both organs were ground to powder using a mortar and pestle in liquid nitrogen, and then lysed in lysis buffer containing 8 M urea, 2 M thiourea, and phosphatase inhibitors (Sigma, Madison, WI, USA). The lysate was sonicated and centrifuged at 10 000 × *g* for 30 min at 4°C, and the resultant supernatant was transferred to a new tube. Proteins were precipitated by addition of three volumes of cold acetone, followed by centrifugation at 8000 × *g* for 30 min at 4°C. The resultant precipitate was dissolved in lysis buffer, reduced with DTT (final concentration, 10 mM), and subsequently alkylated with iodoacetic acid (final concentration, 25 mM).

The resultant protein solution was diluted to 1 M urea in 50 mM NH_4HCO_3 (pH 8.0), and then incubated with trypsin (Promega, Madison, WI, USA) at 37°C for 16 h. The solution

Correspondence: Professor Hisashi Hirano, Advanced Medical Research Center, Yokohama City University, Fukuura 3–9, Kanazawa, Yokohama 236-0004, Japan
E-mail: hirano@yokohama-cu.ac.jp
Fax: +81-45-787-2787

Abbreviations: MOAC, metal oxide affinity chromatography; **MPPD**, *Medicago* PhosphoProtein Database; **FDR**, false discovery rate

was desalted using StageTips with C18 Empore disk membranes (3 M, St. Paul, MN, USA) [9]. Phosphopeptide enrichment based on MOAC was carried out using Titansphere (GL Sciences, Tokyo, Japan) according to the manufacturer's protocol. Before MS analysis, phosphopeptides were desalted using StageTips with C18 Empore disk membranes, and then eluted with 0.1% v/v TFA/50% v/v ACN and dried by evaporation.

Phosphopeptides were resuspended in 0.3% v/v formic acid, and analyzed on an Orbitrap MS (LTQ Orbitrap Velos, Thermo Fisher Scientific, Bremen, Germany). The analytical conditions for the Orbitrap were as follows: LC column: 75 μm × 150 mm, Acclaim PepMap C18, 3 μm, 100 Å (Thermo Fisher Scientific); mobile phase: (A) 0.1% v/v formic acid/2% v/v ACN, (B) 0.1% v/v formic acid/95% v/v ACN; gradient (A:B): 98:2 (0 min), 58:42 (120 min), 0:100 (120–130 min); flow rate: 300 nL/min; mass scan range: m/z 350–1200; mass resolution: 30,000. MS/MS spectra were extracted using the Xcalibur software (version 2.0, Thermo Fisher Scientific).

From the MS and MS/MS data, proteins were identified using the Kazusa DNA Research Institute lotus EST database and the MASCOT software, ver. 2.2.04 (Matrix Science, London, UK). The search parameters were as follows: enzyme, trypsin; peptide mass tolerance, ±5 ppm; MS/MS tolerance, ±0.5 Da; maximum missed cleavages, 2; variable modifications: carbamidomethyl (C), carbamyl (K), carbamyl (N-term), oxidation (M), phospho (ST), phospho (Y); false discovery rate (FDR) <1%. Identified sequences were BLAST-searched using NCBI nonredundant databases. GO analysis was performed using a web application (agriGO; http://bioinfo.cau.edu.cn/agriGO/) [10] using the singular-enrichment analysis tool with the following parameters: background, as suggested for the *L. japonicus* genome; statistical test method, Fisher; multi-test adjustment method, Bonferroni; significance level, 0.01; minimum number of mapping entries, 5.

Quantitation of mRNA was carried out on an Mx3000P real-time PCR system (Stratagene, La Jolla, CA, USA) using the One-step SYBR PrimeScript RT-PCR Kit II (Takara Bio, Shiga, Japan). The level of β-actin mRNA was used for normalization. The forward and reverse primer sets were as follows: ATM-kinase homolog, 5′-TCCTCGAGT AAGCGGAGAAA-3′ and 5′-GCTCAGGACATCCCAAACAT-3′; β-actin, 5′-GCATTGTTGGTCGTCCTCGT-30 and 5′-TGTGCCTCATCCCCAACATA-3′.

Our phosphoproteomic analysis of *L. japonicus* identified 721 phosphopeptides derived from 343 phosphoproteins in cotyledons, and 931 phosphopeptides from 437 phosphoproteins in hypocotyls, with 46.5% overlap between the phosphoproteins identified in the two organs (Fig. 1). GO analysis was performed for 142 phosphoproteins specifically detected in cotyledons and 275 phosphoproteins specific to hypocotyls. This analysis revealed enrichment of the GO term "RNA processing" in hypocotyls, but not in cotyledons. Among the 437 phosphoproteins detected in hypocotyls, 24 were RNA processing related proteins such as mRNA-splicing factors and RNA-binding proteins, indicating that the protein synthesis necessary for differentiation into various organs is upregulated in hypocotyls (Table 1).

We also performed kinase-specific prediction analyses of the cotyledon- and hypocotyl-specific phosphorylation sites (Fig. 1B) using a web application (NetphosK; http://www.cbs.dtu.dk/services/NetPhosK/) [11]. These analyses revealed that different kinases were activated in cotyledons and hypocotyls (Fig. 2A). In particular, many peptides containing ATM-kinase target motifs, X-X-pS/pT-Q-X-X, were detected in cotyledons. A homolog of the gene encoding ATM kinase in *Medicago truncatula* (XM_003601213.1) was identified in *L. japonicus* (clone ID: LjFL3–066-DG12 [5′]). Real-time RT-PCR analysis revealed that expression of the ATM-kinase homolog in cotyledons was ~3.7-fold higher than in hypocotyls (Fig. 2B). ATM kinase is a sensor kinase that responds to DNA damage; when activated, it can cause cell death or regulate the cell cycle via phosphorylation signaling [12]. This finding suggests that this ATM-kinase homolog plays a significant role in the cotyledons of *L. japonicus* seeds.

In recent years, protein phosphorylation, which plays a key role in the signal transduction, has been investigated using proteomic techniques [13, 14]. In those studies, many phosphopeptides were efficiently enriched and purified using enrichment techniques such as IMAC and MOAC. Moreover, upgraded protein databases and highly sensitive, accurate, and high-throughput analytical techniques such as MS have greatly facilitated and accelerated the development of phosphoproteomic research. Additionally, tools for prediction of kinase-specific phosphorylation sites and signal-transduction pathways are available as web applications [15]. These tools allow identification of large numbers of phosphoproteins. Using the IMAC method, Rose et al. [16] identified 3457 unique phosphopeptides from 829 proteins of *M. truncatula* roots, and used these data to construct the *Medicago* PhosphoProtein Database (MPPD). MPPD contains 35 proteins with the ATM-kinase target motif, X-X-pS/pT-Q-X-X. However, the phosphopeptides containing this motif, which we detected in this study, are not present in MPPD. Meyer et al. [17] identified a total of 2001 phosphopeptides from 956 proteins in *Glycine max*, *Brassica napus*, and *A. thaliana* by a combination of the IMAC and MOAC methods. That study identified very few phosphoproteins that were common among those three species, suggesting either that protein phosphorylation is differently regulated depending on species or that detectable phosphoproteins differ greatly depending on the enrichment technique. Meyer et al. also found that phosphotyrosine constituted 7.1, 7.2, and 3.5% of total phosphorylated amino acid residues in developing seeds of *G. max*, *B. napus*, and *A. thaliana*, respectively. The percentage of phosphotyrosine in *A. thaliana* (3.5%) was similar to that reported by Sugiyama et al. [8] in cultured cells of *A. thaliana* (4.3%). Those authors concluded that phosphorylation at tyrosine residues may be prevalent in plants. In our experiments, phosphoserine, phosphothreonine, and phosphotyrosine constituted, respectively, 90.0, 8.5, and 1.5% of the phosphorylated residues in

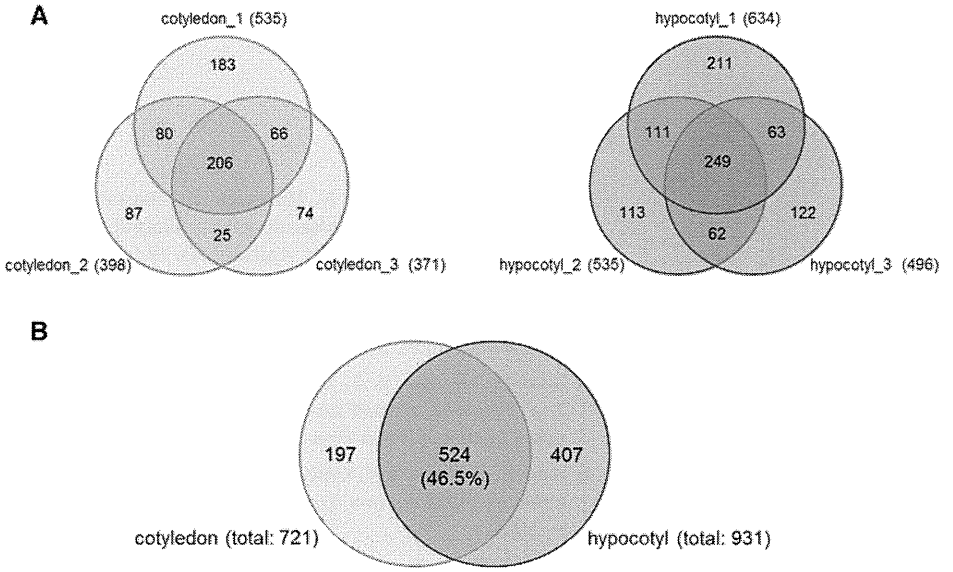

Figure 1. (A) The number of identified peptides in biological triplicates. The measurements were repeated three times to identify phosphopeptides more comprehensively. (B) Overlap between cotyledons and hypocotyls. Proteins were identified at 1% FDR, calculated by a decoy search using the MASCOT software.

cotyledons, and 87.8, 9.8, and 2.4 of the phosphorylated residues in hypocotyls (Fig. 2C). The percentages of phosphotyrosines we observed in *L. japonicus* seeds after water absorption (1.5% in cotyledons and 2.4% in hypocotyls of mature seeds) were considerably lower than those reported by Sugiyama et al.

Legume–rhizobium symbiosis has also been studied using proteomic techniques. In *G. max* root hair, Nguyen et al. [18] detected 273 phosphopeptides that were upregulated by inoculation with *Rhizobium*. Serna-Sanz et al. [19] compared phosphoproteins induced by nodulation factor and flagellin peptide, using 2D polyacrylamide gel electrophoresis.

Table 1. Phosphoproteins involved in RNA processing in hypocotyls

	BLASTP search		
	Protein	Accession no.	Taxonomy
chr2.CM0031.300.nc	Protein argonaute 4 like	gi|356554251	*Glycine max*
chr1.CM0378.200.nd	U2 snrnp auxiliary factor, small subunit	gi|255575357	*Ricinus communis*
LjT48K02.60.nc	Alkylated DNA repair protein alkB homolog 8 like	gi|356508138	*Glycine max*
chr2.CM0018.160.nd	RNA-binding protein 8A like	gi|356497345	*Glycine max*
chr5.CM0200.210.nd	Pre-mRNA processing factor 40 homolog A like	gi|356574333	*Glycine max*
chr2.LjT32G18.130.nc	Heterogeneous nuclear ribonucleoprotein A2 homolog 2 like	gi|356571134	*Glycine max*
chr4.LjT32J05.120.nc	Splicing factor, arginine/serine-rich 13A	gi|357478561	*Medicago truncatula*
chr1.CM0033.20.nd	Arginine/serine-rich splicing factor	gi|255568494	*Ricinus communis*
chr4.CM0042.2070.nc	Pre-mRNA splicing factor SPF27-like protein	gi|357521555	*Medicago truncatula*
chr5.CM0052.230.nd	Polypyrimidine tract binding protein homolog 3 like	gi|356535770	*Glycine max*
chr1.CM0133.1540.nc	Lariat debranching enzyme	gi|357465981	*Medicago truncatula*
chr1.CM0033.10.nd	Arginine/serine-rich splicing factor	gi|255568494	*Ricinus communis*
chr3.CM0135.290.nd	Peter Pan like protein	gi|356544390	*Glycine max*
chr5.CM0260.430.nc	U4/U6 small nuclear ribonucleoprotein Prp3 like	gi|356495750	*Glycine max*
chr3.CM0135.140.nc	RNA-binding protein	gi|357473911	*Medicago truncatula*
chr4.CM0281.160.nc	Protein CWC15 homolog A isoform 2	gi|225461997	*Vitis vinifera*
LjT18N19.10.nd	Heterogeneous nuclear ribonucleoprotein A3 like protein	gi|357475705	*Medicago truncatula*
chr4.CM0172.160.nc	DEAD-box ATP-dependent RNA helicase 30 like	gi|356513635	*Glycine max*
chr3.CM0792.150.nd	Serine/arginine repetitive matrix protein	gi|357472861	*Medicago truncatula*
chr2.CM0405.110.nd	Splicing factor, arginine/serine-rich 13A	gi|357492235	*Medicago truncatula*
chr4.CM0421.390.nc	Lysyl-tRNA synthetase like	gi|356533832	*Glycine max*
LjT39A22.50.nd	Arginine/serine-rich splicing factor RSP40 like	gi|356575923	*Glycine max*
LjT15I01.230.nd	Periodic tryptophan protein like protein	gi|357507105	*Medicago truncatula*
chr2.CM0904.170.nd	Cleavage and polyadenylation specificity factor subunit 2 like isoform 2	gi|356530858	*Glycine max*

Searches for sequence similarity were performed using the BLASTP program.

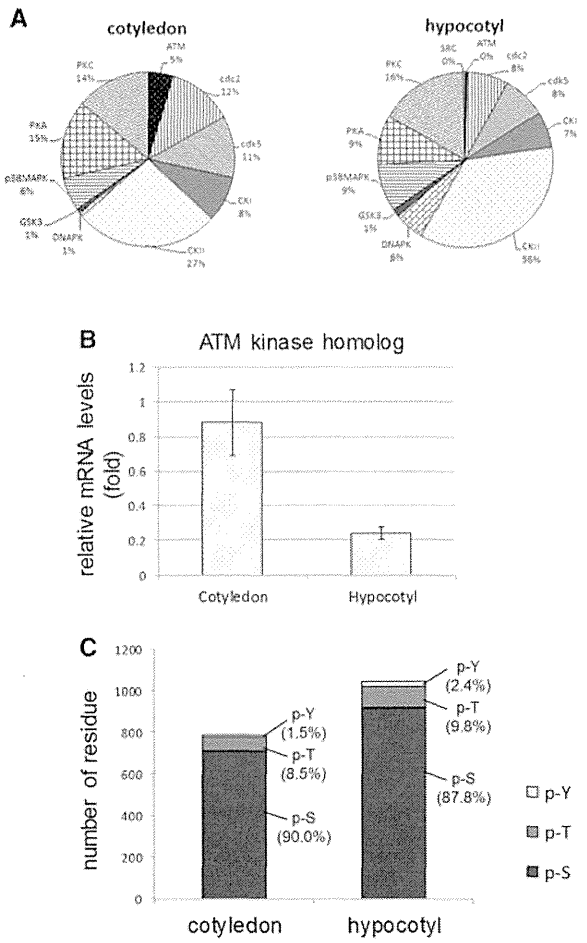

Figure 2. Comparison of phosphorylated sites in cotyledons and hypocotyls. (A) Kinase-specific prediction of phosphorylation sites using a web application. Cotyledon- and hypocotyl-specific phosphopeptides (197 and 407, respectively) were analyzed using NetphosK (http://www.cbs.dtu.dk/services/NetPhosK/). (B) Real-time RT-PCR analysis of the gene encoding ATM kinase. Expression of ATM kinase in cotyledons was ~3.7-fold higher than in hypocotyls. (C) The numbers of p-S, p-T, and p-Y residues in cotyledons and hypocotyls. p-S, phosphoserine; p-T, phosphothreonine; p-Y, phosphotyrosine.

However, those studies did not identify proteins phosphorylated in response to the treatments.

This is the first report of a dataset of phosphoproteins of *L. japonicus* seed cotyledons and hypocotyls. This dataset provides information that will be useful for investigations of seed-germination mechanisms. Furthermore, we expect that the roles of protein phosphorylation during grain filling and seed development could also be investigated using techniques similar to those described here.

The mass spectrometry proteomics data have been deposited to the ProteomeXchange Consortium (http://proteomecentral.proteomexchange.org) via the PRIDE partner repository [20] with the dataset identifier PXD000053 and DOI 10.6019/PXD000053.

The authors have declared no conflict of interest.

References

[1] Umezawa, T., Sugiyama, N., Mizoguchi, M., Hayashi, S. et al., Type 2C protein phosphatases directly regulate abscisic acid-activated protein kinases in *Arabidopsis*. *Proc. Natl. Acad. Sci. USA* 2009, *106*, 17588–17593.

[2] Assmann, S. M., G protein signaling in the regulation of rice seed germination. *Sci. STKE* 2005, *310*, cm12.

[3] Dam, S., Laursen, B. S., Ornfelt, J. H., Jochimsen, B. et al., The proteome of seed development in the model legume *Lotus japonicus*. *Plant Physiol.* 2009, *149*, 1325–1340.

[4] Sato, S., Nakamura, Y., Kaneko, T., Asamizu, E. et al., Genome structure of the legume, *Lotus japonicus*. *DNA Res.* 2008, *15*, 227–239.

[5] Collins, M. O., Yu, L., Choudhary, J. S., Analysis of protein phosphorylation on a proteome-scale. *Proteomics* 2007, *7*, 2751–2768.

[6] Imami, K., Sugiyama, N., Kyono, Y., Tomita, M., Ishihama, Y., Automated phosphoproteome analysis for cultured cancer cells by two-dimensional nanoLC-MS using a calcined titania/C18 biphasic column. *Anal. Sci.* 2008, *24*, 161–166.

[7] Nabetani, T., Kim, Y. J., Watanabe, M., Ohashi, Y. et al., Improved method of phosphopeptides enrichment using biphasic phosphate-binding tag/C18 tip for versatile analysis of phosphorylation dynamics. *Proteomics* 2009, *9*, 5525–5533.

[8] Sugiyama, N., Nakagami, H., Mochida, K., Daudi, A. et al., Large-scale phosphorylation mapping reveals the extent of tyrosine phosphorylation in *Arabidopsis*. *Mol. Syst. Biol.* 2008, *4*, 1–7.

[9] Rappsilber, J., Ishihama, Y., Mann, M., Stop and go extraction tips for matrix-assisted laser desorption/ionization, nanoelectrospray, and LC/MS sample pretreatment in proteomics. *Anal. Chem.* 2003, *75*, 663–670.

[10] Du, Z., Zhou, X., Ling, Y., Zhang, Z., Su, Z., agriGO: a GO analysis toolkit for the agricultural community. *Nucleic Acids Res.* 2010, *38*, W64–W70.

[11] Blom, N., Sicheritz-Ponten, T., Gupta, R., Gammeltoft, S., Brunak, S., Prediction of post-translational glycosylation and phosphorylation of proteins from the amino acid sequence. *Proteomics* 2004, *4*, 1633–1649.

[12] Adachi, S., Minamisawa, K., Okushima, Y., Inagaki, S. et al., Programmed induction of endoreduplication by DNA double-strand breaks in *Arabidopsis*. *Proc. Natl. Acad. Sci. USA* 2011, *108*, 10004–10009.

[13] Kosako, H., Nagano, K., Quantitative phosphoproteomics strategies for understanding protein kinase-mediated signal transduction pathways. *Expert Rev. Proteomics* 2011, *8*, 81–94.

[14] Rigbolt, K. T., Blagoev, B., Quantitative phosphoproteomics to characterize signaling networks. *Semin. Cell Dev. Biol.* 2012, *23*, 863–871.

[15] Kamath, K. S., Vasavada, M. S., Srivastava, S., Proteomic databases and tools to decipher post-translational modifications. *J. Proteomics* 2011, *75*, 127–144.

[16] Rose, C. M., Venkateshwaran, M., Grimsrud, P. A., Westphall, M. S. et al., Medicago PhosphoProtein Database: a repository for *Medicago truncatula* phosphoprotein data. *Front Plant Sci.* 2012, *3*, 122.

[17] Meyer, L. J., Gao, J., Xu, D., Thelen, J. J., Phosphoproteomic analysis of seed maturation in *Arabidopsis*, rapeseed, and soybean. *Plant Physiol.* 2012, *159*, 517–528.

[18] Nguyen, T. H., Brechenmacher, L., Aldrich, J. T., Clauss, T. R. et al., Quantitative phosphoproteomic analysis of soybean root hairs inoculated with *Bradyrhizobium japonicum*. *Mol. Cell. Proteomics* 2012, *11*, 1140–1155.

[19] Serna-Sanz, A., Parniske, M., Peck, S. C., Phosphoproteome analysis of *Lotus japonicus* roots reveals shared and distinct components of symbiosis and defense. *Mol. Plant Microbe Interact.* 2011, *24*, 932–937.

[20] Vizcaíno, J. A. Côté, R. G., Csordas, A., Dianes, J. A. et al., The PRoteomics IDEntifications (PRIDE) database and associated tools: status in 2013. *Nucleic Acids Res.* 2012, doi: 10.1093/nar/gks1262

Journal of proteome research

Article

pubs.acs.org/jpr

Mass Spectrometric Analysis of the Phosphorylation Levels of the SWI/SNF Chromatin Remodeling/Tumor Suppressor Proteins ARID1A and Brg1 in Ovarian Clear Cell Adenocarcinoma Cell Lines

Ayuko Kimura, Noriaki Arakawa, and Hisashi Hirano*

Advanced Medical Research Center and Graduate School of Medical Life Science, Yokohama City University, Fukuura 3-9, Kanazawa, Yokohama 236-0004, Japan

Supporting Information

ABSTRACT: Protein phosphorylation is one of the major factors involved in tumor progression and malignancy. We performed exploratory studies aimed at identifying phosphoproteins characteristic to cell lines derived from ovarian clear cell adenocarcinoma (CCA), a highly malignant type of ovarian cancer. Comparative phosphoproteome analysis revealed that the phosphopeptides of five SWI/SNF chromatin remodeling/tumor suppressor components, including ARID1A and BRG1, were significantly down-regulated in CCA cells. We then quantitatively determined the phosphorylation levels of ARID1A and BRG1 by immunoprecipitation–multiple reaction monitoring (IP–MRM) that we used for analysis of the cognate phospho- and nonphosphopeptides of low-abundance proteins. The phosphorylation level of Brg1 at Ser1452 was down-regulated in CCA cells, whereas the phosphorylation level of ARID1A at Ser696 did not significantly differ between CCA and non-CCA cells. These results were consistent with the results of immunoblotting showing that Brg1 levels were comparable, but ARID1A levels were lower, in CCA cells relative to non-CCA cells. This is the first report to demonstrate reduced phosphorylation of Brg1 in CCA-derived cells. Our data also indicated that the IP–MRM/MS method we used is a powerful tool for validation of the phosphoproteins detected by shotgun analysis of phosphopeptides.

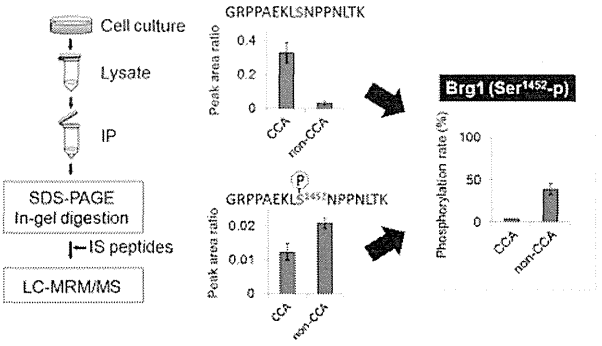

KEYWORDS: *phosphorylation, ovarian cancer, clear cell adenocarcinoma, multiple reaction monitoring, ARID1A, Brg1*

INTRODUCTION

Reversible protein phosphorylation is a critical mechanism involved in regulation of various cellular processes, including intracellular signaling and protein–protein interaction. Aberrant phosphorylation and dephosphorylation of proteins are among the major causes of tumorigenesis and cancer malignancy. Therefore, phosphoproteome analysis provides information that cannot be obtained by analyses of tumor samples at the genome, exome, or proteome levels. Recent advances in methods for enrichment of phosphopeptides allow the comprehensive identification and quantitation of phosphopeptides, enabling the discovery of dozens or hundreds of phosphopeptides that are up- or down-regulated in various biological samples by a single LC–MS run.[1] To interpret quantitative differences in phosphopeptide levels, however, it is important to distinguish between up- or down-regulation caused by changes in phosphorylation level and that caused by changes in protein levels. Protein phosphorylation level is usually confirmed using antiphosphopeptide antibodies. In some cases, it is also possible to perform MS-based quantitation of phosphorylation levels by detecting phosphopeptides along with their cognate nonphosphopeptides. In particular, this is possible when (1) the target protein and its phosphopeptides are present at relatively high levels[2−5] or (2) the target protein is overexpressed, or its phosphorylation level has been augmented by treatment with a phosphatase inhibitor or activation of an upstream signaling pathway.[6−8] Multiple reaction monitoring (MRM)–MS utilizing two stages of mass filters (Q1, Q3) also effectively increases the selectivity and sensitivity of phosphopeptides detection.[3,5−7,9,10] However, vast numbers of phosphorylation sites that are up- or down-regulated under specific conditions still have not been confirmed because of technical limitations on detection of the native phosphorylation state of low-abundance proteins. In this study, we sought to identify histological subtype-specific phosphoproteins in a particular type of cancer by comprehensive phosphoproteome analysis. Concurrently, we used a highly sensitive method for quantitation of the native phosphorylation state of proteins using MRM–MS.

Ovarian clear cell adenocarcinoma (CCA) is a highly malignant type of epithelial ovarian carcinoma. CCA differs

Special Issue: Proteomics of Human Diseases: Pathogenesis, Diagnosis, Prognosis, and Treatment

Received: May 12, 2014
Published: August 1, 2014

from the other major histological subtypes of epithelial ovarian carcinoma in its histological, biological, and clinical properties,[11−13] resulting in a poorer prognosis and higher resistance to antitumor drugs (e.g., cisplatin). Therefore, to effectively manage this disease, it is necessary to develop much more effective therapeutic strategies. Several extensive studies at the transcriptome and proteome levels have identified many molecular signatures of CCA (e.g., mutations in the *PIK3CA*, *KRAS*, and *PPP2R1A* genes; up-regulation of IL6, HNF-1β, VCAN, ANX4, and TFPI2; methylation of TMS-1/ASC; and loss of PTEN)[14−17] and also revealed the extensive molecular heterogeneity of this disease. Recent genome-wide and exome-sequence analyses also revealed frequent somatic mutations in the AT-rich interactive domain−containing protein 1A (*ARID1A*) gene in around half (46−57%) of CCA tumors.[18−20] These mutations, distributed throughout the coding region of *ARID1A* were accompanied by significant down-regulation of its protein product.[18,20] Although *ARID1A* mutation is predicted to be one of the major triggers of CCA development, it is not applied to the half of CCA that exhibits positive expression of ARID1A. These molecular signatures of CCA as well as some phenotypes related to the high malignancy of CCA (e.g., resistance to antitumor drugs) are also inherited in a heterogeneous manner in some CCA-derived cell lines.[12,18,21−23] Although the characteristic features of CCA have been extensively studied at the transcriptome and proteome levels, to date, no published study has analyzed CCA at the phosphoproteome level.

In this study, we performed a phosphoproteomic study aimed at revealing novel molecular signatures of CCA, using CCA-derived cell lines with or without known molecular signatures of CCA. As a result, we observed CCA-specific down-regulation of phosphorylation of an ARID1A-associated component, Brahma protein homologue 1 (BRG1), by combining comparative phosphoproteome analysis and IP−MRM/MS-based confirmation of protein phosphorylation levels using cell lines derived from CCA and other histological subtypes of epithelial ovarian carcinoma. The data also indicated that the highly sensitive IP−MRM/MS method we used concurrently for the analysis of phosphorylation levels of low-abundance phosphoproteins is a powerful tool for validation of phosphoproteins detected by shotgun analysis of phosphopeptides.

MATERIALS AND METHODS

Cell Culture

The ovarian cancer cell lines, OVTOKO, OVISE, MCAS, OVKATE, OVSAHO, OVMANA, OVSAYO, OVCAR-3, RMG-I, and RMG-II were cultured as previously reported.[24] JHOC5, JHOC7, and JHOC8 were obtained from RIKEN (Tsukuba, Japan) and cultured in 1:1 DMEM:HamF12 (Nacalai Tesque, Kyoto, Japan) supplemented with 10% FBS (Gibco, Carlsbad, CA) and 0.1 mM nonessential amino acids (NEAA; Nacalai Tesque). ES-2 cells were purchased from ATCC (Manassas, VA) and cultured in McCoy's 5A medium (Gibco) supplemented with 10% FBS.

Protein Extraction, Trypsin Digestion, And Phosphopeptide Enrichment

Cells were grown to 70−80% confluence on 15 cm dishes. To obtain cell lysates, the cells were sonicated on ice four times for 30 s each at 28 kHz using a Sonic UR-21P (Tomy, Japan) in denaturation buffer (20 mM HEPES [pH 8.0], 9 M urea, 25 mM sodium pyrophosphate, 10 mM beta-glycerophosphate) supplemented with phosphatase inhibitor cocktails 1 and 2 (Sigma, Madison, WI). Cleared cell lysate was obtained by centrifugation at 10 000*g* for 30 min at 4 °C. A total of 100 μg of cleared cell lysate from two biological replicates of each cell line was reduced with 10 mM dithiothreitol and alkylated with 10 mM iodoacetamide. After dilution with 3 volumes of 20 mM HEPES, proteins were digested with 1:20 (enzyme/substrate w/w) of trypsin (Promega, WI) at 37 °C for 14 h. The digested mixture was acidified with 1% trifluoroacetic acid (TFA). Peptides were desalted using StageTips filled with C18 Empore disc membranes and SDB (3M, St. Paul, MN). Phosphopeptides were enriched using the Titanosphere Phos-TiO kit (GL Science, Tokyo, Japan). After desalting with StageTips, peptides were evaporated in a vacuum concentrator, then dissolved in 2% acetonitrile/0.1% formic acid for the MS analysis.

Shotgun LC−MS/MS and Differential Analysis of Peptide Profiles

Phosphopeptides were separated on a C18 reversed-phase column with a linear gradient of acetonitrile (4−40%) for 145 min and then analyzed on an LTQ-Orbitrap MS (Thermo Fisher Scientific). Full-scan MS spectra (m/z 350−1200) were acquired in positive-ion electrospray ionization mode. Each of the 15 most intense ions in the full-scan MS spectrum was subjected to subsequent CID product ion scan with normalized collision energy (35%). The spray voltage was set to 1.7 kV, and the capillary temperature was set to 250 °C. Quantitative analysis was performed using the Progenesis LC−MS software (v3.1; Nonlinear Dynamics, Newcastle upon Tyne, U.K.). Retention times of all samples were aligned using one LC−MS run as a reference. Features with a charge of +2, +3, or +4 were selected, and the experimental variations of each sample were normalized against all features in all samples. Samples were separated into two groups, CCA and non-CCA, and the groups were then compared by multivariate statistical analysis. Peptide identification was performed by searching for the corresponding amino-acid sequences in the UniProtKB database (http://www.uniprot.org/) using the Mascot software (v.2.3.02, Matrix Science, London, U.K.) with 3 ppm of peptide mass tolerance and a tolerance of 0.5 Da for MS/MS fragmentation ions. Peptide assignment was reimported to the original precursor ion signals with calculated normalized abundances. The list of peptides with ion score >30 as the cutoff, using a significance threshold of $p < 0.05$ and analysis of variance (ANOVA) p value <0.01, was used to search for the characteristic pathways for each group using DAVID Bioinformatics Resources 6.7.[25,26]

Immunoblot Analysis and Immunoprecipitation

Cells were grown to 70−80% confluence on 15 cm dishes. To obtain cell lysates, we sonicated the cells at 4 °C in extraction buffer (20 mM Tris-HCl [pH 7.4], 150 mM NaCl, 2 mM EDTA, 1% Triton-X 100) supplemented with phosphatase inhibitor cocktail 3 (Sigma) and protease inhibitor cocktail (Nacalai Tesque). Cleared cell lysate was obtained by centrifugation at 10 000*g* for 30 min at 4 °C. Proteins were cleared and concentrated by acetone precipitation. Then, proteins were separated by SDS-PAGE on 5−20% gradient gels, and the resolved proteins were transferred onto PVDF membranes. ARID1A and Brg1 proteins were detected by using antibodies PSG3 (sc-32761) and G-7 (sc-17796) (both from Santa Cruz Biotechnology, CA), which recognize amino acids 600−1018 of ARID1A and 209−296 of Brg1, respectively.

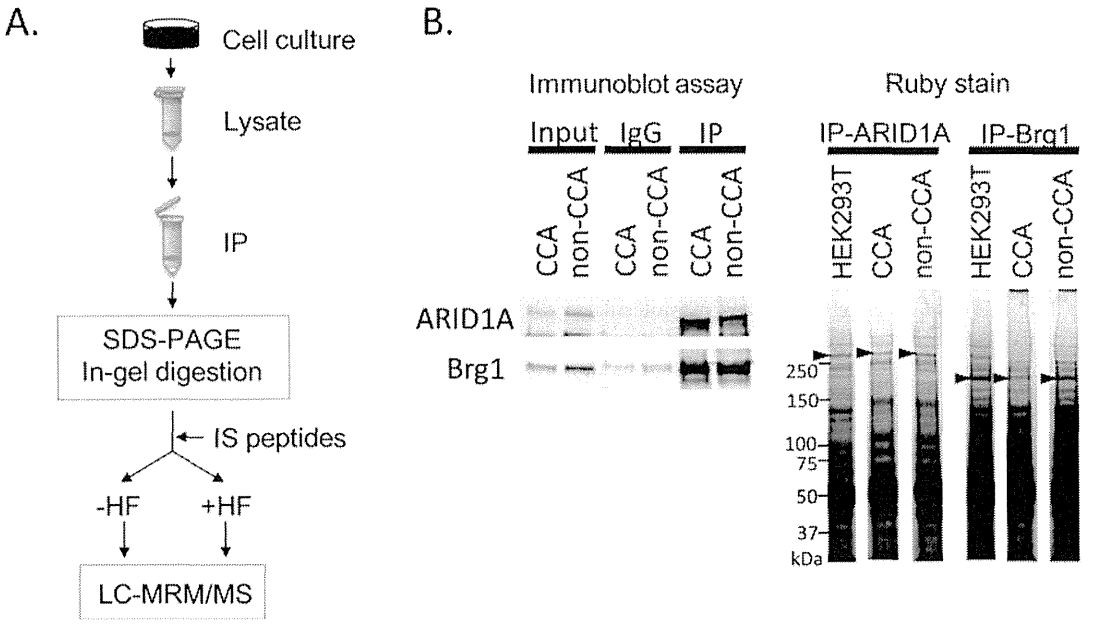

Figure 1. IP–MRM/MS analysis of phosphopeptides. (A) Protocol overview. ARID1A and Brg1 proteins were immunoprecipitated from cell lysates and then resolved by SDS-PAGE. Protein bands corresponding to ARID1A and Brg1 were excised and subjected to in-gel trypsin digestion. Samples spiked with IS phospho- and nonphosphopeptides were analyzed by LC–MRM/MS. Detection was also confirmed by chemical dephosphorylation of samples containing spiked IS peptides by HF treatment. (B) Immunoprecipitation of ARID1A and Brg1. IP-enriched proteins were separated by SDS-PAGE and detected by SYPRO Ruby staining (right) and immunoblotting (left). Protein bands corresponding to ARID1A and Brg1 (indicated by arrows) were excised from the gel for subsequent MRM analysis.

ARID1A and Brg1 were immunoprecipitated from lysate containing 1 mg total protein by incubation at room temperature for 1 h on a microtube mixer with 2 μg of the appropriate antibody. Antigen–antibody complex was collected with 200 μL of antimouse IgG Dynabeads magnetic beads (Life Technologies, Carlsbad, CA). The antigen–antibody reaction was performed before the incubation with anti-IgG resin because preincubation of anti-IgG resin with the antibodies significantly decreased the resultant yield of target proteins. ARID1A and Brg1 were further purified by the SDS-PAGE to improve the sensitivity of phosphopeptide detection: after the beads were washed three times with extraction buffer and twice with phosphate-buffered saline (PBS), proteins were eluted with 2× SDS sample buffer, separated on 5–20% gradient gels, and stained with SYPRO Ruby (Life Technologies). Protein bands corresponding to ARID1A (~270 kDa) and Brg1 (~190 kDa) were excised and subjected to in-gel digestion with trypsin, followed by desalting with StageTips for LC–MRM/MS analysis (Figure 1). Lysates from three biological replicates of each cell line were used for the analysis.

LC–MRM/MS Analysis

Target peptides for MRM were chosen by MRM–EPI scanning of phosphopeptides detected by the comprehensive phosphoproteome analysis and their cognate nonphosphopeptides, using a Qtrap 5500 LC-MS/MS system (AB Sciex, Framingham, MA). Two each MRM transitions with Q1 and Q3 set to low-resolution and total scan cycle time <2.0 s were selected for each peptide based on the maximum peak intensity of initially selected transitions by MRMpilot (AB Sciex) (Supplementary Table 1 in the Supporting Information). Peptides were separated on a C18 reversed-phase column with a linear gradient of acetonitrile (5–40%) for 45 min at 200 nL/min and then analyzed on a Qtrap 5500 LC–MS/MS system in MRM mode. Corresponding phospho- and nonphosphopeptide pairs for each phosphorylation site were analyzed in parallel in the same LC–MS run. Quantitation was performed using MultiQuant (AB Sciex, ver2.0.2). Linear detection of internal standard (IS) peptides (Scrum Corporation) was confirmed between 10 and 500 fmol (Supplementary Figure 1A in the Supporting Information). Detection of phosphorylation rate was tested using mixtures of the IS phospho- and nonphosphopeptides at different phospho/nonphosphopeptide (p/n) ratio (4:1, 2:1, 1:1, 1:2, and 1:4) (Supplementary Figure 1B in the Supporting Information). Phosphopeptide peak area was corrected by dividing the original peak area by the average p/n ratio of IS peptides, as calculated from the standard curves: 2.34 ± 0.13 for Brg1 (Ser1452-p) and 1.06 ± 0.16 for ARID1A (Ser696-p). Phosphorylation rate was calculated as follows

$$[\text{phosphorylation rate } \%] = A/(A + B)^* \times 100$$

*A = corrected peak area of phosphopeptide
B = peak area of nonphosphopeptide

For analysis of trypsin digests of immunoprecipitated proteins, peptides prepared from 0.25 to 0.5 mg of lysate proteins were mixed with 100 fmol each of the IS phospho- and nonphosphopeptides. MRM signals derived from the lysate proteins were verified by coelution with stable isotope–labeled IS peptides, dephosphorylation by incubation with 50% hydrofluoric acid (HF) overnight at 4 °C, and MRM–EPI analysis.

RESULTS

Comparative Phosphoproteome Analysis Using CCA and Non-CCA Cells

Comparative phosphoproteome analysis was performed on cell lysates from six CCA (RMGI, RMGII, OVISE, OVTOKO, OVSAYO, and OVMANA) and four non-CCA (MCAS, OVCAR-3, OVSAHO, and OVKATE) ovarian cancer cell

Table 1. Immunoblot Detection and Mutation Status of ARID1A and Brg1

histological subtype	cell line	ARID1A protein	ARID1A gene	Brg1 protein	Brg1 gene	ref	cell line used in: phosphoproteomic analysis	immunoblot	MRM (ARID1A)	MRM (Brg1)
CCA	RMGI	+	WT	++	WT	16, 24	×	×	×	
	ES2	++	WT	++	WT	16, 24		×	×	×
	JHOC5	+	WT	−	N/A	16		×	×	
	JHOC7	+	WT	++	N/A	23		×		
	JHOC8	−	N/A	+	N/A	23		×		
	RMGII	−	c.5251-8delAGCAAGGT	++	N/A	this study	×	×		
	OVISE	−	c.608dupA, c.1626-7delGC	++	WT	16, 24	×	×		×
	OVTOKO	−	c.289C>T, c.6625delC	++	WT	16, 24	×	×		
	OVSAYO	−	c.6718-26del	++	N/A	this study	×	×		
	OVMANA	−	c.1332C>T, c.6791C>G	+	N/A	14, 16	×	×		×
non-CCA	MCAS	++	WT	++	N/A	23	×	×	×	×
	OVCAR3	++	WT	++	WT	21, 25	×	×	×	×
	OVSAHO	++	N/A	++	WT	26	×	×		
	OVKATE	++	N/A	++	WT	26	×	×		

[a]++: high or medium; +: low; −: signal not detected; WT: wild type; N/A: data not applicable; ×: cell line used in the analysis.

Table 2. Biological Pathways in BioCarta Related to the Proteins with Down-Regulated Phosphopeptide Levels in CCA (Pathway Enrichment by DAVID)[a]

term	count	%	*P* value	genes	fold enrichment
vdrPathway:Control of Gene Expression by Vitamin D Receptor	8	2.1	1.0×10^{-5}	TOP2B, BAZ1B, **SMARCC2**, SNW1, NCOR1, **SMARCC1, ARID1A, BRG1 (SMARCA4)**	9.3
hSWI-SNFpathway:Chromatin Remodeling by hSWI/SNF ATP-dependent Complexes	5	1.3	1.5×10^{-3}	**SMARCC2, SMARCC1, ARID1A, BRG1 (SMARCA4), POLR2A (RPB1)**	9.2
integrinPathway:Integrin Signaling Pathway	6	1.6	3.4×10^{-3}	BCR, VCL, TLN1, PXN, TNS1, ZYX	5.5
cell2cellPathway:Cell to Cell Adhesion Signaling	4	1.1	4.0×10^{-3}	VCL, PXN, CTNNA1, CTNNB1	11

[a]SWI/SNF components are indicated by bold.

lines (Table 1). A total of 16 305 integrated peaks from these samples were aligned and quantitated using the Progenesis LC–MS software. Peptides were identified by MASCOT search against the Uniprot database. A total of 1086 peptides with MASCOT score >30 were subjected to multivariate statistics analysis of peptide up- or down-regulation, resulting in the identification of 620 phosphopeptides with ANOVA p value <0.01. Next, the protein list was subjected to pathway enrichment analysis using DAVID Bioinformatics Resources 6.7[25,26] to clarify the biological relevance of the detected phosphopeptides in CCA and non-CCA cell lines. Pathway-based classifications obtained from the BioCarta database with p value <0.05 detected four pathways (Table 2), comprising 17 proteins detected with decreased phosphopeptide levels in the analysis described above (Figure 2 and Supplementary Figure 2 in the Supporting Information). Two of these pathways, involved in the control of gene expression (control of gene expression by vitamin D receptor and chromatin remodeling by hSWI/SNF ATP-dependent complexes), share four SWI/SNF components: ARID1A, Brg1, SMARCC1, and SMARCC2. The other two pathways are involved in cell-adhesion signaling (integrin signaling pathway and cell-to-cell adhesion signaling). These phosphorylation sites conserved the consensus phosphorylation motif of CMGC family kinases (cyclin-dependent kinases [CDKs], mitogen-activated protein kinases, glycogen synthase kinases, and CDK-like kinases) as detected by Motif-X[27,28] and NetPhosK[29] (Supplementary Figure 3 in the Supporting Information), indicating the possible involvement of this family of kinases in CCA development. The annotated tandem mass spectra of these peptides are shown in Supplementary Figure 4 in the Supporting Information.

Phosphopeptides of the tumor suppressor protein ARID1A as well as four proteins that along with ARID1A form the SWItch/Sucrose NonFermentable (SWI/SNF) chromatin remodeling complex, Brg1 (SMARCA4), SMARCA1, SMARCA2, and RPB1, were significantly down-regulated in CCA cell lines (Table 3, Figure 2) relative to non-CCA cell lines. Although down-regulation of some SWI/SNF components has been reported in various types of tumors, including CCA,[20,30−32] previously no information was available about the phosphorylation levels of these proteins in cancer cells/tissues. Therefore, we focused our study on the phosphorylation status of the two most frequently down-regulated components of SWI/SNF complex, ARID1A, and Brg1.

Protein Levels of ARID1A and Brg1 in CCA and Non-CCA Cells

To distinguish down-regulation of protein levels from reduction in phosphorylation levels, we compared the levels of ARID1A and Brg1 among 10 CCA and 4 non-CCA cell lines by immunoblot assay. The cell lines used in each analysis are indicated in Table 1. Expression of both ARID1A and Brg1 was observed in all four non-CCA cell lines tested, whereas random down-regulations of these proteins were observed in the CCA cell lines (Figure 3 and Table 1): ARID1A was not detectable in RMG-II, JHOC8, OVISE, OVTOKO, OVSAYO, and OVMANA cells, and Brg1 was not detectable in JHOC5 cells. The presence or absence of ARID1A in this analysis was consistent with available information regarding mutations of the

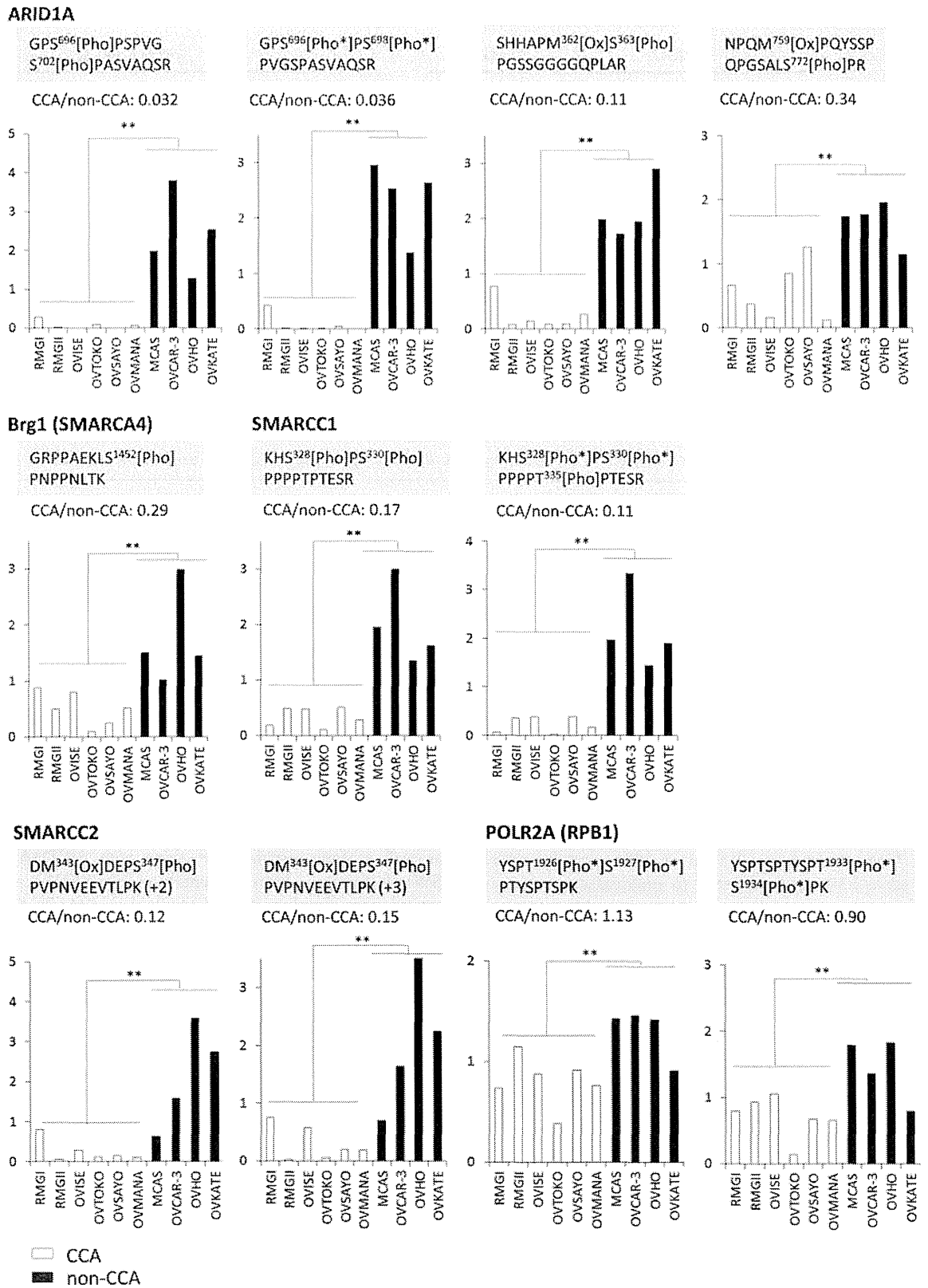

Figure 2. Phosphopeptides of SWI/SNF components detected in CCA and non-CCA cells. Relative peak intensities, normalized against the average peak intensities of all samples, are shown. Bars represent the means of duplicate samples. Phosphopeptides of five SWI/SNF components (ARID1A, Brg1, SMARCC1, SMARCC2, and RPB1) were down-regulated in CCA cells relative to non-CCA ovarian cancer cells ($p < 0.01$), as revealed by shotgun LC-MS analysis of phosphopeptides. Significant differences between the CCA and non-CCA groups are indicated by asterisks (**: $p < 0.01$). Ambiguously identified phosphorylation sites are indicated by [Pho*].

ARID1A gene[18,20,21,33−35] (Table 1). These results indicate that the CCA cell-line-specific alterations of the phosphopeptide levels of ARID1A, as observed in the comprehensive phosphoproteome analysis, were not due to down-regulation

dx.doi.org/10.1021/pr500470h | J. Proteome Res. 2014, 13, 4959−4969

Table 3. Phosphopeptides Down-Regulated in CCA (hSWI/SNF Complex-Related Proteins)[a]

Uniprot ID	gene	description	sequence	charge	score	expect	max fold	Anova
O14497	ARID1A	AT-rich interactive domain-containing protein 1A	GPS[696][Pho]PSPVGS[702][Pho]PASVAQSR	2	36.2	4×10^{-4}	32	8.6×10^{-5}
			GPS[696][Pho*] PS[698][Pho*]PVGSPASVAQSR	3	34.7	3×10^{-3}	28	4.8×10^{-5}
			SHHAPM[362][Ox]S[363][Pho] PGSSGGGGQPLAR	3	51.1	4×10^{-5}	8.8	3.0×10^{-7}
			NPQM[759][Ox] PQYSSPQPGSALS[772][Pho] PR	3	30.4	2×10^{-3}	2.9	6.9×10^{-4}
P51532	BRG1 (SMARCA4)	probable global transcription activator SNF2L4	GRPPAEKLS[1452][Pho]PNPPNLTK	3	37.0	1×10^{-3}	3.4	3.2×10^{-4}
Q92922	SMARCC1	SWI/SNF complex subunit SMARCC1	KHS[328][Pho*] PS[330][Pho*]PPPPT[335][Pho]PTESR	2	41.1	3×10^{-4}	9.4	9.3×10^{-6}
			KHS[328][Pho]PS[330][Pho]PPPPTPTESR	3	39.3	2×10^{-4}	5.7	3.3×10^{-7}
Q8TAQ2	SMARCC2	SWI/SNF complex subunit SMARCC2	DM[343][Ox]DEPS[347][Pho]PVPNVEEVTLPK	2	53.7	5×10^{-5}	8.6	9.6×10^{-6}
			DM[343][Ox]DEPS[347][Pho]PVPNVEEVTLPK	3	34.8	7×10^{-4}	6.8	1.6×10^{-4}
P24928	POLR2A (RPB1)	DNA-directed RNA polymerase II subunit RPB1	YSPT[1926][Pho*]S[1927][Pho*]PTYSPTSPK	2	75.0	2×10^{-7}	1.6	4.3×10^{-3}
			YSPTSPTYSPT[1933][Pho*]S[1934][Pho*]PK	2	57.0	5×10^{-64}	2.0	9.0×10^{-3}

[a]Phosphorylation sites are indicated by [Pho], ambiguously identified phosphorylation sites are indicated by [Pho*], and oxidation sites are indicated by [Ox].

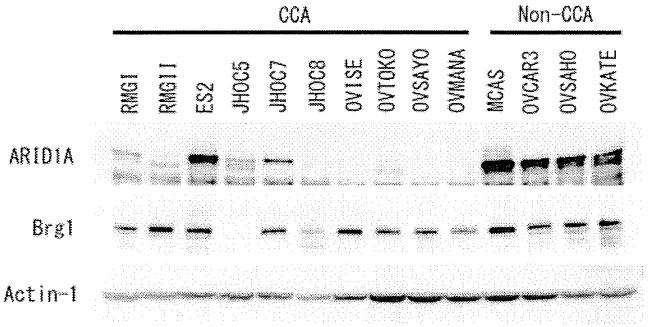

Figure 3. Immunoblot analysis of ARID1A and Brg1. ARID1A was not detectable in six CCA cell lines (RMG-II, JHOC8, OVISE, OVTOKO, OVSAYO, and OVMANA), whereas Brg1 was not detectable in one CCA cell line (JHOC5). By contrast, positive expression of ARID1A and Brg1 was confirmed in all four non-CCA cell lines tested (MCAS, OVCAR3, OVSAHO, and OVKATE). Equal protein loading was confirmed by immunoblotting for Actin-1.

of phosphorylation but were instead due to reductions in the protein level. By contrast, it is more likely that phosphorylation level of Brg1 was altered in the CCA cell lines.

LC–MRM/MS-Based Quantification of the Phosphorylation Levels of ARID1A and Brg1

Next, to verify the phosphorylation levels of ARID1A and Brg1 in CCA and non-CCA cell lines, we used the LC–MRM method for quantitation of phosphorylation levels by direct analysis of their phospho- and nonphosphopeptides (Figure 1). The phospho- and nonphosphopeptide pairs containing the phosphorylation sites of Brg1 (at Ser1452) and ARID1A (at Ser696), which were detected by comprehensive phosphoproteome analysis with subsequent assignment by MRM-EPI analyses (MASCOT score >40, Supplementary Figure 4 in the Supporting Information), were chosen for subsequent investigations.

The phosphorylation rate of ARID1A and Brg1 was measured using proteins purified from HEK293T cells, which express both proteins at high levels. Peptide samples were spiked with a mixture of IS phospho- and nonphosphopeptides mixture and separated into two tubes (Figure 4). Peptide dephosphorylation was performed by adding HF to one of these tubes and incubating overnight at 4 °C. As shown in Figure 4A,B, MRM signals for both IS and internal phosphopeptides of Brg1 (Ser1452-p) and ARID1A (Ser696-p) almost disappeared following the HF treatment. By contrast, signals for IS nonphosphopeptides of these proteins exhibited a slight increase, likely due to the dephosphorylation of IS phosphopeptides. Internal nonphosphopeptides of Brg1 and ARID1A exhibited a further increase after HF treatment. Amino-acid sequences of phospho- and nonphosphopeptides detected by MRM were also confirmed by MRM-EPI scan detecting these proteins with MASCOT score >40. These results demonstrated successful detection of the target phosphorylation sites based on the shift of phosphopeptide peaks into the corresponding nonphosphopeptide peaks following dephosphorylation by HF treatment.

Next, we analyzed the phosphorylation levels of Brg1 in CCA and non-CCA cells, using the pooled cell lysates spiked with 100 fmol per run of each IS peptide, in triplicate samples (Figure 5). CCA cells with positive expression of Brg1 (OVISE, OVMANA, and ES-2 cells) and non-CCA cells (MCAS and OVCAR-3) (Figure 3) were used for this analysis. The level of the phospho-Ser1452 peptide of Brg1 was 2 times lower in the CCA pool, whereas that of its cognate nonphosphopeptide was 10 times higher in the CCA pool relative to the non-CCA pool (Figure 5B, left). The phosphorylation rate of this site was calculated to be 3.6% in CCA cells and 39% in non-CCA cells, a greater than ten-fold decrease in CCA cells (Figure 5C, left).

The level of the phospho-Ser696 peptide of ARID1A was two times lower in the ARID1A-positive CCA pool (RMG-I, ES-2, and JHOC5) relative to the non-CCA pools (MCAS and OVCAR-3) (Figure 5B, right). The corresponding nonphosphopeptide of ARID1A was also present at lower levels in CCA cells than in non-CCA cells, showing a pattern similar to that of the phosphopeptide. The phosphorylation rate of the phospho-Ser696 peptide of ARID1A was calculated to be 86% in CCA pool and 88% in the non-CCA pool, with no significant differences between CCA and non-CCA cells (Figure 5C, right).

DISCUSSION

In this study, we observed reduced phosphorylation of the well-studied tumor suppressor protein Brg1 in CCA-type ovarian cancer cell lines. To make this observation, we used the IP–MRM/MS method to detect the native phosphorylation level of low-abundance proteins in combination with shotgun LC–MS analysis of phosphopeptides. This approach might also be

A. Brg1

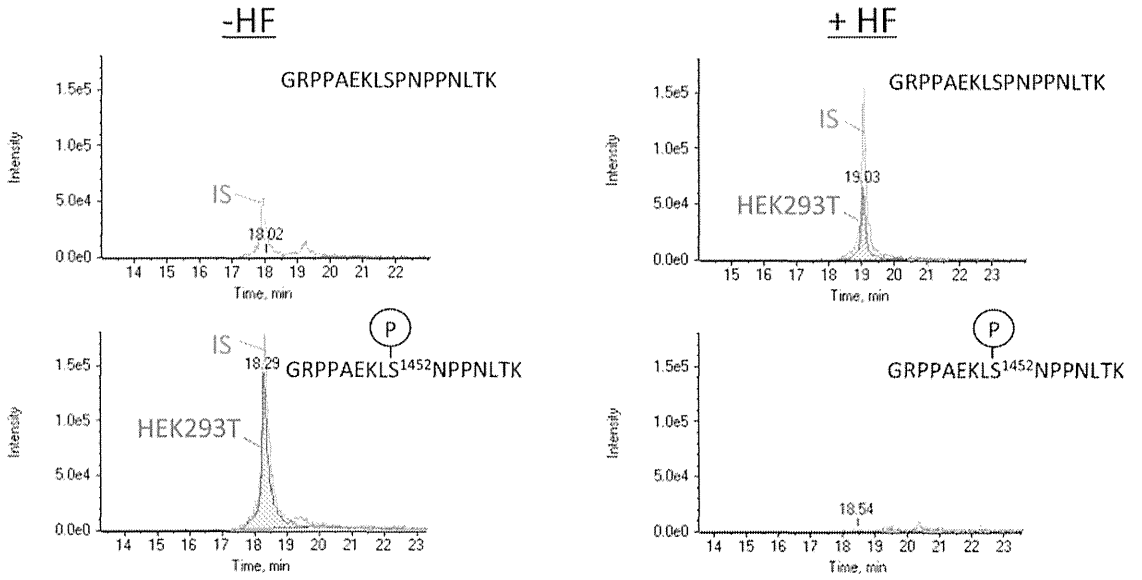

B. ARID1A

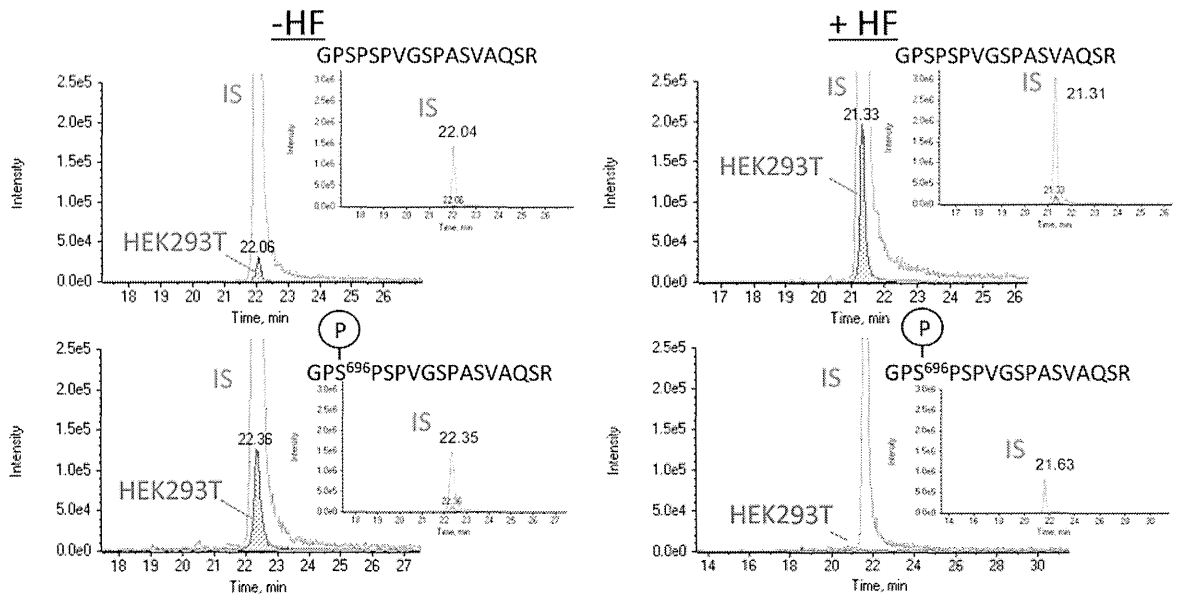

C.

Protein	Peptide	Average peptide peak area (x10^6)			
		HEK293T		IS	
		- HF	+ HF	- HF	+ HF
Brg1	GRPPAEKLSPNPPNLTK	0.0032	0.81	0.79	2.1
	GRPPAEKLS^{1452}[Pho]PNPPNLTK	2.4	0.0087	3.3	0.058
ARID1A	GPSPSPVGSPASVAQSR	0.35	2.5	15	37
	GPS^{696}[Pho]PSPVGSPASVAQSR	1.9	0.0092	24	13

Figure 4. Confirmation of the detection of intracellular phospho-/nonphosphopeptides of Brg1 and ARID1A. (A,B) Peptide samples prepared from HEK293T cells spiked with IS phospho- and nonphosphopeptides were treated overnight with or without HF at 4 °C. Significant reductions in the signals for the IS and internal phosphopeptides were observed following dephosphorylation by HF treatment, whereas the signals for the IS and internal nonphosphopeptides increased. (C) Average peptide peak area of phospho- and nonphosphopeptides of ARID1A and Brg1, calculated from the results of two independent experiments.

dx.doi.org/10.1021/pr500470h | J. Proteome Res. 2014, 13, 4959−4969

A.

Protein	Peptide	Average peptide peak area (x10^6)				Peak area ratio	
		Sample		IS		Sample/IS	
		CCA	non-CCA	CCA	non-CCA	CCA	non-CCA
Brg1	GRPPAEKLSPNPPNLTK	0.55	0.045	1.2	1.3	0.33	0.034
	GRPPAEKLS^{1452}[Pho]PNPPNLTK	0.052	0.096	1.7	1.9	0.012	0.021
ARID1A	GPSPSPVGSPASVAQSR	0.029	0.062	6.9	6.9	0.46	0.76
	GPS^{696}[Pho]PSPVGSPASVAQSR	0.23	0.31	8.9	9.1	2.8	6.3

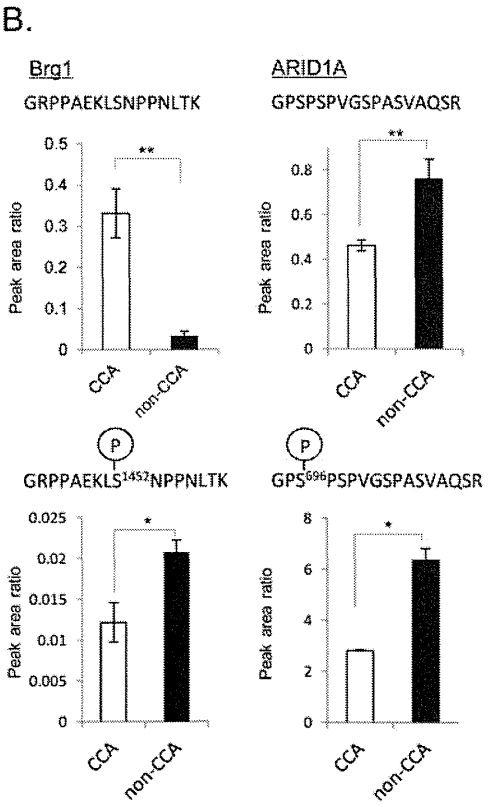

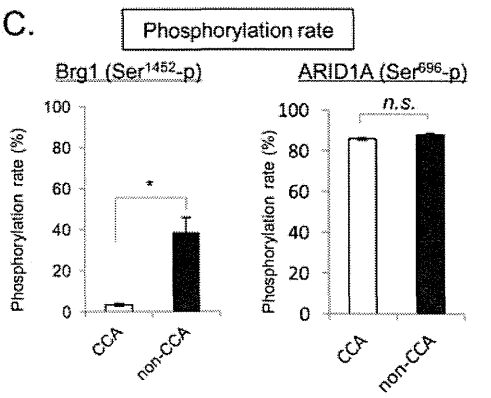

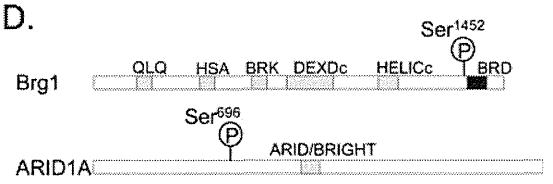

Figure 5. IP–MRM/MS analysis of the phosphorylation levels of Brg1 and ARID1A in CCA and non-CCA cells. (A) Average peak area of phospho-/nonphosphopeptides. Results were obtained from three independent experiments. Peak area ratio was also calculated by dividing the average peak area of the internal peptide by the area of the IS peptide. (B) Bar graphs of the peak area ratio of phospho-/nonphosphopeptides. Error bars denote standard deviations. Significant differences are indicated by asterisks (**: $p < 0.01$, *: $p < 0.05$). (C) Phosphorylation rate (%) calculated from the peak area ratio. Error bars denote standard deviations. Significant differences are indicated by asterisks (*: $p < 0.05$) (D) Schematic domain structure of human Brg1 and ARID1A, as predicted by SMART.[42] The phosphorylation site of Brg1 (Ser1452) resides in the region proximal to the bromodomain, whereas that of ARID1A (Ser696) resides in a region with unknown function.

useful for other functionally important but low-abundance phosphoproteins to reveal the roles of controlled protein phosphorylation in various biological processes.

The sensitivity of MRM/MS-based detection of phospho- and nonphosphopeptides can be increased by improving the purity of target proteins. MRM analysis of phosphopeptides is sometimes challenging because essentially only one peptide covers each phosphorylation site of a given protein. In addition, the MS peak intensity of phosphopeptides is usually very low relative to that of the cognate nonphosphopeptides due to